IMPACTS AND VEGETATION-INDUCED ATTENUATION OF WIND- AND VESSEL-GENERATED WAVES

by

Rachel Schaefer

A thesis submitted to the Faculty of the University of Delaware in partial fulfillment of the requirements for the degree of Honors Bachelor of Civil Engineering with Distinction

Spring 2019

IMPACTS AND VEGETATION-INDUCED ATTENUATION

OF WIND AND VESSEL GENERATED WAVES

by

Rachel Schaefer

Approved: ____
Dr. Jack Puleo, Ph.D.
Professor in charge of thesis on behalf of the Advisory Committee

Approved: ____
Dr. Thomas McKenna, Ph.D.
Committee member from the Department of Geological Sciences

Approved: ____
Dr. Sue McNeil, Ph.D.
Committee member from the Board of Senior Thesis Readers

Approved: ____
Dr. Earl Lee II, Ph.D.
Deputy Faculty Director, University Honors Program

ACKNOWLEDGMENTS

I would like to thank my family and friends for supporting my interests and goals every step of the way. I thank my twin sister Serena especially for introducing me to engineering in high school. I thank Dr. Jack Puleo for being an inspirational teacher, researcher, and advisor. I could not have done this without fellow undergraduate senior Mike Larner. Thank you to Dr. Tom McKenna for helping with the field experiment and being my second reader. Thank you to Dr. Sue McNeil for asking thought-provoking questions and being my third reader.

Thank you to Janelle Skaden, Shannon Brown, Demetra Cristaudo, Ben Gross, Stan Borrell, Liangyi Yue, Emily Tulsky, and James Holyoke for assisting with the field experiment.

Thanks to the University of Delaware Department of Civil and Environmental Engineering for the Chair's Senior Thesis Fellowship. Thank you to the University of Delaware Undergraduate Research Program for Conference and Travel Expense funding. Thank you to the Delaware Department of Natural Resources and Environmental Control for providing access to Pea Patch Island and allowing us to conduct the field study. Thanks to the University of Delaware Center for Applied Coastal Research for providing equipment and supplies.

TABLE OF CONTENTS

LIST OF TABLES

LIST OF FIGURES

ABSTRACT

Rising sea levels due to climate change combined with increasing economic activity along coastal areas necessitate effective coastal defenses. Ships laden with heavy cargo can generate large wave groups that may erode shorelines. Pea Patch Island, the home of Fort Delaware and a major wading bird nesting site located on the Delaware River, suffers from beach erosion and wetlands loss. The Delaware River attracts an array of cargo ships which generate large ship wakes. Riprap installed on part of the island's shoreline absorbs and reflects wave energy, but increases erosion at the ends of the riprap structure. On shorelines without riprap, vegetation attenuates wave energy by inducing drag on the water, thus reducing erosion rates. Two studies were conducted simultaneously from June 6 to July 9, 2018 on the island to determine the effects of ship wakes on the east and west sides of the island and how vegetation in the retreating western wetlands attenuates ship wakes. Ultrasonic distance meters, pressure sensors, and current meters were deployed in cross-shore transects to obtain water depths, and cross-shore and alongshore water velocities. Time-lapse cameras recorded daytime imagery of ship passages and wakes. At the western marshy site. the vegetation patch was composed of *Phragmites australis* and *Schoenoplectus pungens*. Measured plant characteristics and site elevation profiles were used to explore potential impacts on hydrodynamics. Total wind wave energy exceeded total ship wake energy during the month-long deployment, but the ship wake energy was more heavily concentrated. The relative contributions of wind-generated waves increased landward along the transect. Vegetation more effectively attenuated high frequency significant wave heights than low frequency significant wave heights. *Phragmites australis* was shown to effectively attenuate wave energy flux by at least 30%.

Chapter 1

INTRODUCTION

1.1 Pea Patch Island

Climate change is threatening coastal communities and environments. Global mean sea level is expected to rise at least 1 meter (m) by 2100 (Neumann et al., 2015). Climate change has been linked to increasing frequency and intensity of storm evens (DeLaune and White, 2012). Sea level rise can also increase shoreline erosion and wetland migration rates. The built and natural environments and human health will become increasingly susceptible to these hazards. Tidal wetlands provide a buffer mechanism against coastal hydrodynamic forcing. About 39% of the population lives near the coastline (Ache et al., 2015), with about 80% of the coastline consisting of tidal wetlands (Titus, 1998). Yet, tidal wetlands are not immune to sea level rise and storms, and as wetlands migrate inland they can be squeezed out by human development along coastal areas.

Pea Patch Island, located on the Delaware River about 1.4 kilometers (km) off of Delaware City and about 1.6 km offshore of Fort Mott State Park (Figure 1), is ecologically and historically important. The island is about 1.9 km in length and 0.8 km across at its widest points, with a total area of about 1.04 km^2. Although the island is small, it is the home of Fort Delaware (Figure 2) and the largest wading bird nesting area on the East Coast north of Florida, with 12,251 nesting pairs in 1993 down to 3,886 nesting pairs in 2000 (United States Army Corps of Engineers, 2009). Pea Patch Island is the largest heronry on the Atlantic Coast (Coxe, 2012). The State of Delaware runs regular tours to Fort Delaware, hosting about 30,000 visitors every year (United States Army Corps of Engineers, 2009). Protecting the low-lying island is of interest to the Delaware Department of Natural Resources and Environmental Control (DNREC). The main aims of this project are to explore the impacts of wind- and ship-generated waves on the western side of Pea Patch Island and the effects of wetlands vegetation in attenuating these waves.

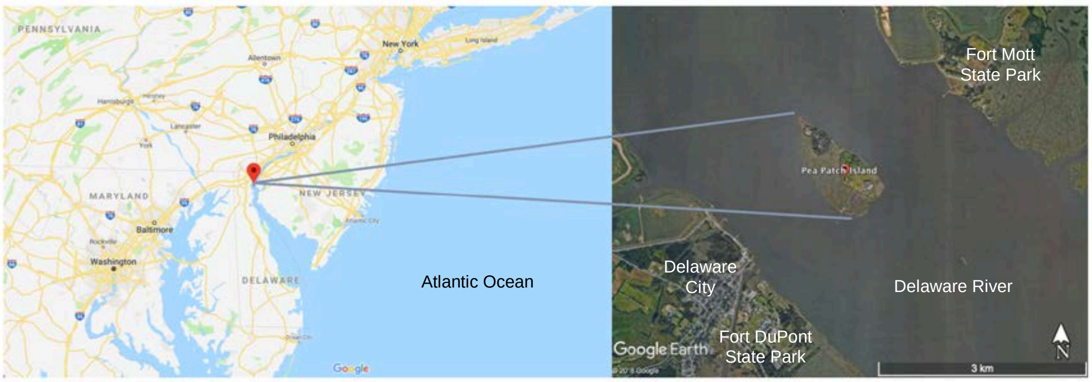

Figure 1: Location of Pea Patch Island on the Delaware River.

Figure 2: Photograph of the front of Fort Delaware (taken by Evan Krape).

The riprap seawall built along the eastern edge of Pea Patch Island helps protect the historic fort from erosion but deprives the shoreline farther south of sediment. Waves diffracting around the southern end of the riprap combined with the lack of sediment caused the loss of marsh at the end of the riprap (Figure 3). The progression of images also shows reduction in total wetlands area, a loss of marsh habitat.

Figure 3: Erosion over time on Pea Patch Island, with Fort Delaware shown. a) Erosion due to wave diffraction in riprap seawall gap. b) Stone wall gap was fixed after erosion nearly reached the moat around Fort Delaware; wetlands loss west of the riprap seawall. c) Continued erosion and loss of wetlands west of the riprap seawall due to reduced alongshore sediment transport.

An understanding of the morphological history of the island sets the stage for evaluating wave impacts. According to Coxe (2012), Pea Patch Island began as a mud bank in the Delaware River in the 1700s. At some point a cargo ship carrying peas grounded on the mud bank, lending the island its name. The low-lying island used to flood at every high tide, but its strategic position on the Delaware River led the government to seize the island and begin placing fill, building embankments and digging drainage ditches in 1813-1814. Construction began on a fort on the island in

1815, made difficult by the low elevation. The first fort was eventually destroyed by fire and replaced by 1863, in time for the Civil War. At that time, it was used to hold Confederate Army prisoners. Within 10 years of construction, the rebuilt fort was declared obsolete. In the 1890s the fort was modernized and in the early 1900s the United States Army Corps of Engineers pumped sand onto the island to protect it from flooding. After World War II, the island was turned into a Delaware state park (United States Army Corps of Engineers, 1997).

In the 1970s, the embankment along the southeastern side of Pea Patch Island failed, causing severe erosion (United States Army Corps of Engineers, 1997). Beginning in 1999, the Army Corps of Engineers rebuilt the seawalls around the island. These activities were mainly directed to protect the island from erosion due to a dredging project to deepen the Delaware River to accommodate larger vessels (United States Army Corps of Engineers, 2009). In total, about 823 m of riprap seawall were built and 384 m of historical riprap seawall were rebuilt (United States Army Corps of Engineers, 2010). Though the area behind the riprap is protected from erosion, the western wetlands are unprotected and may experience increased loss due to the hardened armoring project and the resulting reflected waves and reduced alongshore sediment transport and sea level rise.

Soils on Pea Patch Island (Figure 4) consist of Broadkill Mucky Peat (0.59 km^2), Othello Silt Loam (0.18 km^2), Endoaquepts and Sulfaquepts (0.11 km^2), and Urban Land-Othello Complex (0.010 km^2). The peat soil makes up the vast majority of the island, reaching far along the western edge of the island and part of the eastern side. In 1954, the largest marsh communities on Pea Patch Island were pickerelweed tidal marsh and cattail brackish tidal marsh, while today it is mostly reed tidal marsh.

Invasive *Phragmites australis* make up the majority of the current reed marsh. At least three quarters of the current marsh will be flooded by 0.5 m of sea level rise, and all marsh communities will be flooded with 1.5 m of sea level rise (Coxe, 2012).

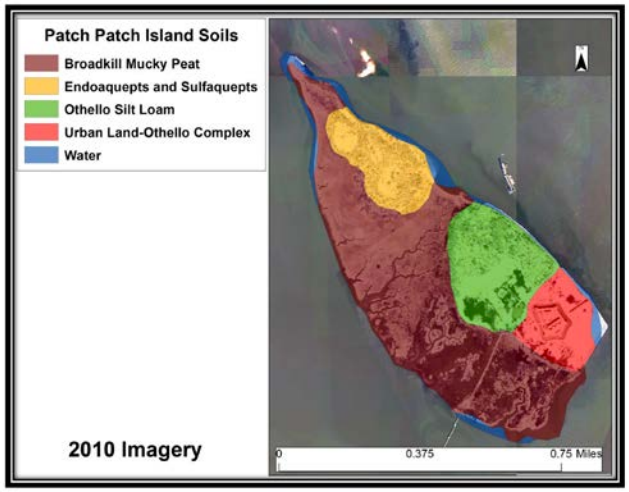

Figure 4: 2010 Pea Patch Island soil map (Coxe, 2012).

1.2 Wind- and Vessel-Generated Waves

Wind blowing in varying directions at varying speeds over water can transfer energy to the water by the formation of waves. These waves can eventually break on and impact shorelines. Wind wave characteristics depend on how long the wind event lasts and over what distance, or fetch, the wind travels. Wind waves occur throughout the day and depend on the local environmental, climate, and weather conditions. Meanwhile, cargo ships, ferries, and other vessels navigate rivers, usually on fixed schedules and in predetermined directions. The Delaware River, for example, is a major shipping channel for Philadelphia, Pennsylvania; Wilmington, Delaware; Camden, New Jersey; and Trenton, New Jersey, located between 15 and 115 km upriver from Pea Patch Island. As vessels move through the river, they displace water, forcing it to flow in front of, around, and under the hull from bow to stern. Ships can thus be represented as moving surface pressure disturbance patches (Soomere, 2006). These initial pressure disturbances propagate as waves away from ships, known as ship wakes. Ship wakes can generally be distinguished from wind-generated waves by several characteristics.

A typical ship wake usually consists of a group of low frequency waves followed by high-frequency large-amplitude waves, as well as an ultra-low-frequency infragravity wave component (Herbert et al., 2018). Torsvik et al. (2015) found that the typical ship wake includes a sliding-frequency chirp signal due to divergent waves and a constant frequency signal due to transverse waves, in addition to nonlinear precursor solitary waves, leading waves, and low-frequency waves. These signals can be found through use of spectrograms, and are common for both large conventional ships and fast ferries.

Under specific conditions, the characteristics of ship wakes follow similar patterns. According to Fang et al. (2011), the wake immediately surrounding and behind a ship is complex, depending on the shape, speed, and propulsion of the ship. Beyond about three ship lengths behind the ship, the ship wake is more predictable, consisting of a turbulent foamy wake and a Kelvin wake. The theoretical Kelvin wake pattern is made up of transverse waves, which cross the ship's track, and divergent waves, which move outward approximately parallel to the ship's track. These waves form a wedge shape with a half angle of 19.5° in deep water conditions. In reality, Kelvin wake angles are often narrower than expected, especially when deep water conditions are not satisfied. The wake structure and angle are dependent on the dimensionless Froude number, the ratio of inertial forces to gravity:

$$F_r = \frac{U}{\sqrt{gh}}, \tag{1}$$

which is based on ship velocity U, the acceleration due to gravity g, and a length h. For a depth-based Froude number, h is the water depth, while for a hull-based Froude number h is the ship hull length. For Froude numbers less than 1, or subcritical flow, the wake structure follows the Kelvin pattern, adhering more closely to it for Froude numbers below 0.5. Such lower Froude numbers would require a low ship velocity or high water depth or ship hull length. For Froude numbers greater than 1, or supercritical flow, the wake narrows, possibly to the point of wave crests travelling almost collinear with the ship direction. Wind-generated wave speed and direction can impact the structure of a ship wake.

Ship wakes, due to their higher energy content relative to wind-generated waves, have the potential to cause higher levels of erosion along coasts (Soomere et al., 2009; Verney et al., 2007; Soomere, 2006). By measuring backscatter signals, which corresponded to sediment concentrations in the water, Herbert et al. (2018) found a peak 43% increase in sediment suspension during the first group of waves within a ship wake, followed by a drop and then another increase that lasted for multiple minutes. They note that increased sediment suspension from ship wakes can damage oyster larvae and feeding activities by stymying their movement and damaging their gills, and also reduce nearshore vegetation growth.

Hofmann et al. (2008) found seasonal and diurnal effects on the relative impacts of ship- and wind-generated waves. In their study of Lake Constance in Germany, ship-generated waves may increase during the summer months in areas where tourist passenger ships are common, while wind-generated waves are fairly consistent throughout the year. Ship-generated waves are less frequent at night when there are fewer passenger ships.

The Delafort Ferry, operated by the Delaware River and Bay Authority, travels on a mostly regular schedule during the visiting season (late April through late September, with other events throughout the year) between Delaware City, Pea Patch Island, and Fort Mott State Park. A work boat brings employees to and from the island on a regular basis as well. It is expected that wakes generated by the ferry and work boat are not large relative to those of cargo ships, but they occur more frequently so may impact the shoreline of Pea Patch Island. The ferry provides mostly regular interval ship wake events that can be compared across tidal cycles. Ship size and speed, as indicated by the hull-based Froude number, can affect how a ship wake propagates. The Delafort Ferry is smaller than typical cargo ships along the Delaware River, and is not meant to carry heavy cargo. While the speeds could not be directly measured, through the use of time-lapse camera frames, the Delafort Ferry appears to travel faster than typical cargo ships. As such, the Delafort may or may not share wake similarities to the larger cargo ships traveling along the Delaware River.

1.3 Vegetation-Induced Attenuation of Waves

Possible options for reducing the impact of ship wakes on shorelines is to implement coastal protection infrastructure. These can come in the form of hardened structures such a stone walls or breakwaters, establishment of natural vegetation or oyster reefs, or using a hybrid approach that attempts to combine the advantages of hardened and natural methods. Many laboratory studies have been conducted on the ability of vegetation to attenuate wave energy; fewer field studies have been done on the topic. Vegetation can be emergent, where the vegetation canopy height exceeds the water level, or submerged, where the vegetation canopy height lies below the water level. Vegetation stems can be rigid or flexible, wherein rigid stems can absorb more force but break more easily, while flexible stems bend under force, allowing more water to flow past (Feagin et al., 2015). As a submerged plant stem bends, the frontal volume of the vegetation decreases, lowering the drag induced on the flow (Luhar and Nepf, 2013).

For a dense patch of emergent vegetation, the drag induced by the vegetation exceeds the drag induced by viscous and turbulent stresses (Lightbody and Nepf, 2006). Lightbody and Nepf (2006) present a momentum balance equation reduced to a balance between vegetation-induced drag and pressure terms, using a quadratic function for the drag force on plant stems and assuming steady, uniform, and fully developed flow with a hydrostatic pressure distribution:

$$\frac{1}{2} C_D a u^2 = g \frac{\partial \eta}{\partial x}, \tag{2}$$

The surface slope is represented by $\frac{\partial \eta}{\partial x}$, C_D is the drag coefficient, a is the frontal area of vegetation per unit volume, g is the acceleration due to gravity, and u is the horizontal fluid velocity. The frontal area of vegetation per unit volume is represented as (Luhar and Nepf, 2013):

$$a = n_b b, \tag{3}$$

where n_b is the number of blades per unit bed area and b is the width of the blade. The drag coefficient is dependent on the Reynolds number (Re_d), the ratio of inertial to viscous forces (Lightbody and Nepf, 2006):

$$Re_d = \frac{ud}{\nu}, \tag{4}$$

where d is the stem diameter and ν is the kinematic viscosity of water. Both a and the stem diameter d are functions of depth above the bed. The vertical variation in vegetation density can help resolve the vertical variation in horizontal velocity (Lightbody and Nepf, 2006).

There are important distinctions between the drag coefficient C_D for individual stems and for entire patches of vegetation. The drag coefficient of a single stem depends on stem morphology and mechanical properties (James, 2004). According to Nepf (1999), the drag coefficient of a patch, also known as the bulk drag coefficient $\overline{C_D}$, depends on the stem density. The wake of an upstream stem can limit the drag coefficient of the trailing stem behind, an effect that increases as stem density increases. Overall, as the stem density and frontal stem volume increases, the bulk drag coefficient would be expected to decrease. This reduced drag effect on wake interactions accumulates across a dense array of stems.

A temporally and spatially averaged drag coefficient can be described as the following (Tanino and Nepf, 2008):

$$C_D = \frac{\langle f_{D-} \rangle}{\rho \langle \bar{u} \rangle^2 \langle d \rangle / 2}, \tag{5}$$

where $\langle f_{D-} \rangle$ is the average drag in the direction of mean flow per unit stem length, ρ is the fluid density, $\langle \bar{u} \rangle$is the fluid velocity in the direction of mean flow averaged over the stem spacing, and $\langle d \rangle$ is the characteristic stem width.

For dense patches of emergent vegetation, the velocity u over the water depth can be approximated as follows (Luhar and Nepf, 2013):

$$u = \sqrt{\frac{2gS}{C_D a}}, \tag{6}$$

where the slope S is the gradient in water depth h and bed elevation z_b in the streamwise (x) direction (Luhar and Nepf, 2013):

$$S = \frac{\partial(h+z_b)}{\partial x}, \tag{7}$$

The turbulence generated by stem wakes is greater than that induced by bed shear stress, with the turbulence intensity increasing with bulk population density (Nepf, 1999). Viscous stress and bed drag are considered negligible relative to vegetation-induced drag (Nepf and Vivoni, 2000). Vegetation in itself reduces bed stress and baffles the flow, trapping sediments and pollutants (Nepf, 2012). The reduction of near-bed stress also reduces particle resuspension (Lightbody and Nepf, 2006).

By inducing drag on the flow of water, vegetation stems attenuate wave energy. The attenuation ability depends on a variety of factors, including the vegetation species, average density, stem height, stem width, stem strength, stem rigidity, leaf height, leaf width, and season (Nepf, 2012; Quartel et al., 2007). Some plant species may lose and gain biomass or die as environmental conditions change, thereby affecting wave attenuation ability.

Attenuation is also inherently dependent on the root system of a plant, whereby a strong network of roots or rhizomes anchor plants to the soil. Many plants have symbiotic relationships with vesicular-arbuscular mycorrhizal fungi (AMF), where the fungi improve drought tolerance, increase nutrient uptake, and lower salt stress, while binding soil together to reduce erosion (Feagin et al., 2015).

Anderson and Smith (2014) found from double-peaked water wave spectra that emergent vegetation preferentially dissipates high-frequency waves compared to low-frequency waves. In addition to reducing the impact of breaking waves, by reducing wave height, vegetation patches can effectively reduce the chances of waves breaking and eroding shorelines (Knutson et al., 1982).

The accumulation of decaying plant material over time into layers of peat material can counter erosion and sea level rise (Gedan et al., 2011). The aforementioned ability of plants to trap sediment can also contribute to the overall accretion of salt marshes. The top litter layer of dead plant material can also increase mineral deposition (Rooth and Stevenson, 2000). If the rate of accretion exceeds the rate of sea level rise, the marsh becomes better protected against climate change.

Peat platforms are subject to erosion. Schwimmer (2001) studied marsh erosion rates and styles at sites along Delaware Bay and Rehoboth Bay. He found that the muddy portion beneath the active root depth erodes faster than the top of the peat scarps, leading to rootmat overhangs and eventual toppling. Marsh erosion can consist of cleft and neck formation, neck separation, and rootmat undercutting. Marsh erosion is thought to be mainly caused by wave action, and strongly correlated with wave power.

During a field study involving ship wakes and *Spartina alterniflora* marshes in Chesapeake Bay, Virginia, Knutson et al. (1982) found 40% and 60% reductions in wave height and wave energy, respectively over the first 2.5 m into a vegetation and 94% reduction in wave height and 100% reduction in wave energy over the first 30 m into vegetation.. These results are from waves generated by a vessel angled relative to the shoreline so as to produce nearly shore-parallel waves.

The variation in vegetation species and the importance of the roots in how vegetation attenuates wave energy makes field studies an attractive option. However, in fields studies a researcher cannot control the slope, vegetation characteristics, or surrounding environment. There are many factors at play, and no variables can be effectively isolated or controlled. The results cannot be easily attributed to any specific factors. Field studies are expensive and logistically difficult to carry out, making the repetition of them throughout the year to compare results a challenging endeavor.

Even so, extensive field studies are not needed to confirm that established vegetation can stabilize shorelines. In 1928 Mr. Wescoat, prompted by coastal erosion, planted over 1 km of *Spartina alterniflora* on his shoreline on the north shore of Wescoat Cove in the Chesapeake Bay, the first example of using marsh vegetation to stabilize the shore in the United States (Knutson et al., 1982).

Many of the parameters described above can be difficult to effectively isolate or calibrate in the field, as compared to the laboratory. Yet the laboratory does not fully replicate the environmental conditions in the field. Field studies are also often necessarily done at the patch scale. As laboratory studies can be done at the stem scale, the canopy scale, and the patch scale, field and laboratory experiments can complement each other. This project involved a field experiment, focusing on the effects of wind- and ship-generated waves on Pea Patch Island and how the wetlands vegetation on the island attenuates these waves.

Chapter 2

METHODS

2.1 Study Area

A field experiment was conducted for 32 days from June 6 to July 9, 2018 on Pea Patch Island. A team visited Pea Patch Island on April 20, 2018 to assess the island and scout out potential study sites. The chosen study sites were on an unvegetated beach on the eastern side and in the wetlands area on the western side of the island (Figure 5). Figure 6 includes photographs of the western marsh site, which is the focus of this paper, from the April visit. The Delaware Department of Natural Resources and Environmental Control (DNREC) provided transportation between Delaware City and Pea Patch Island. Trips to the island were limited to weekdays when large crowds of visitors were not expected and between 7 AM and 2 PM.

At the western site, an approximately cross-shore transect was established with six data collection stations. Each station included a structure made from steel and aluminum pipes and attached sensors. Water depths and velocities were obtained from data collected by instruments along the transect.

Figure 5: Aerial photograph of Pea Patch Island showing the locations of the chosen study sites and the dock used by the Delafort ferry.

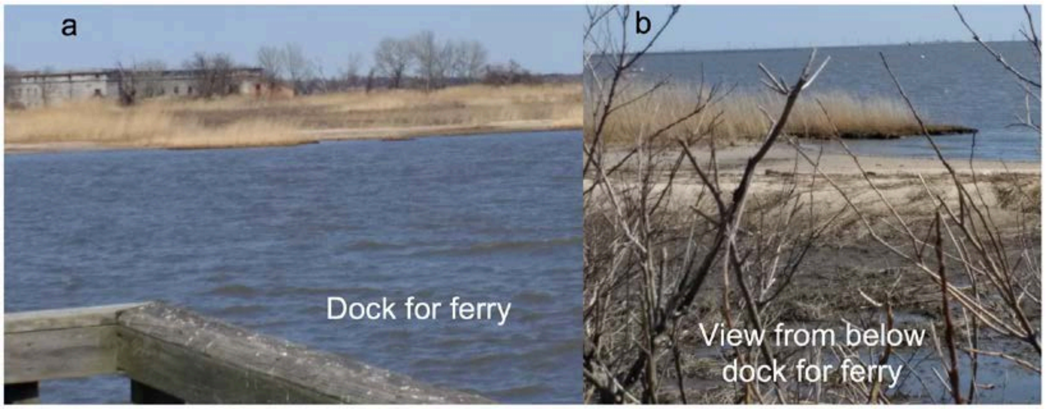

Figure 6: Photographs of western marsh site taken during the visit on April 20, 2018 a) from the dock used by the Delafort ferry offshore and b) from below the dock used by the Delafort ferry, focusing on the vegetation patch of interest.

At the western marsh site, the transect spanned from offshore into a patch of vegetation on an elevated peat terrace (Figure 6b). This peat terrace resembled the type of “neck” formation described by Schwimmer (2001). Near the site, there were multiple “stacks” of separated marsh platform necks eroded away from the main marsh shoreline. The six data collection stations were labelled R0 through R5, with R0 being the most riverward station and R5 being the most landward location (Figure 7). The dock for the Delafort Ferry ran almost parallel to the study transect, and allowed physical access to the site. Station R3 was placed just riverward of the peat platform edge. Station R4 was placed on top of the platform at the interface between patches of *Phragmites australis and Schoenplectus pungens*. and *Phragmites australis*. Station R5 was placed farther into the patch of *Schoenoplectus pungens*. The transect setup is shown in Figure 8. Farther inland, the soil in the vegetation patch became too swampy to effectively deploy a data collection station; otherwise, station R5 or an additional data collection station could have been placed at the landward end of the vegetation patch.

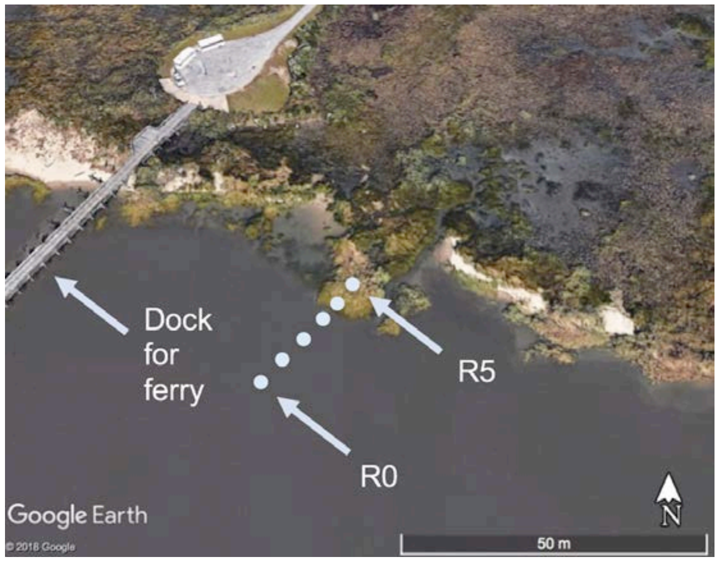

Figure 7: Overhead view of western side of Pea Patch Island with data collection transect, showing necks in the wetlands along the shoreline and an unvegetated sandy area to the west

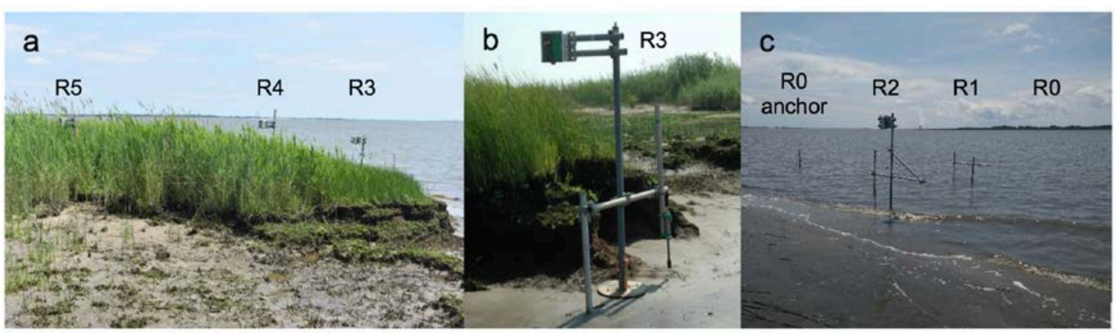

Figure 8: Data collection transect on western side of Pea Patch Island: a) From left to right: R5 through R3; b) R3 in front of peat terrace edge; c) From left to right: R2 through R0 (R0 submerged, connected to lone pipe at left).

Ideally both studies would have been performed side by side, one with a control transect along unvegetated beach and another with a transect into a nearby patch of vegetation along that same beach. The bare beach location on the east side of the island was already preferred as a study site, and while there were patches of vegetation nearby, they were blocked by crumbling seawalls or located in areas that would make deployment and reaching sensors difficult.

2.2 Data Collection

Due to the soft, muddy soils at the site, the steel pipes driven into the ground at each station were prone to rotation and sinking. Wooden boards were cut to fit around the pipes and sit on the bed, while steel grates were zip tied to the pipes and forced underground to try counteracting these issues. Despite this, the scaffolding steel pipe at R1 rotated about 180 degrees over night between June 7 and June 8, and so during the next visit on June 14 secondary steel pipes were driven into the ground and attached to the main pipe at stations R1, R2, and R3 to further improve stability.

Banner Engineering U-GAGE ultrasonic distance meters (UDMs, Figure 8a), RBR solo^{3}D wave16 pressure gauges (Figure 8b), JFE Advantech Co., Ltd. INFINITY-EM AEM-USB custom two-dimensional electromagnetic current meters (ECMs, Figure 8c), and a Nortek Vector three-dimensional acoustic Doppler velocimeter (ADV, Figure 8d) were used to obtain water depths and velocities. “Intensive” studies were done June 18 through June 21 and June 29 through July 2, where some sampling rates were increased from their “regular” levels during the rest of the study.

Station R0 contained the ADV and a pressure gauge. Station R1 contained an ECM running and a pressure gauge. Stations R2 and R3 each included an UDM, ECM, and pressure gauge. R4 had an UDM and pressure gauge. Station R5 had an UDM and two pressure gauges, one of which was set high up on the scaffolding pipe, above the reach of the water, to measure atmospheric pressure. Figure 9 shows station R3 as an example.

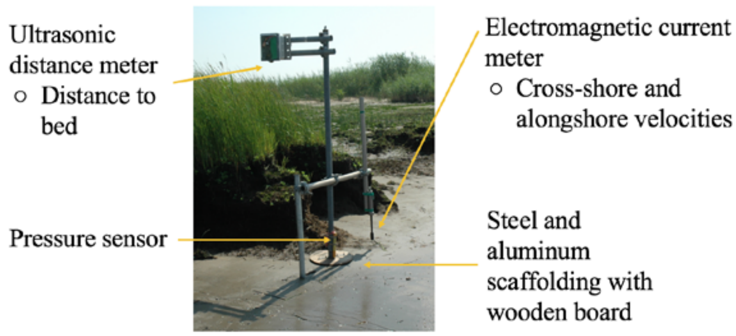

Figure 9: Photograph of station R3 with sensors labelled.

All pressure gauges were set to run at 16 Hertz (Hz) continuously. The ADV was programmed for 16 Hz for 30-s bursts every 5 minutes (min) throughout the study and collected velocity data. The ECMs, which also collected velocity data, were run at 5 Hz for 3-min bursts every 15 min for the “regular” parts of the study and at 5 Hz continuously for the “intensive” parts of the study. The UDMs, which measured distance to the first object acoustic pulses emitted by the sensor hit, usually the water or bed, were run at 2 Hz continuously for the “normal” parts of the study and 4 Hz continuously for the “intensive” parts of the study. Instrument parameters were chosen based on predicted battery life and memory storage and the next anticipated return to the island. The Vector current meter, ECM, and pressure gauges were self-logging.

Figure 8: Instruments used in study: a) Banner Engineering U-GAGE UDM, sealed with bulkhead, inserted through hole in bottom of waterproof box; b) RBR solo^{3}D wave16 pressure gauge diaphragm; c) JFE Adventech Co., Ltd. INFINITY-EM AEM-USB ECM probe; d) ADV probe.

Madgetech Volt101A data loggers were used to store data collected by the UDM. Each logger sensor lithium polymer battery was contained in a waterproof box, with the UDM poking through a hole sealed with a bulkhead in the bottom and positioned so as to point downward (Figures 8a, 9). The watertight boxes were attached to steel plates held to the main steel scaffolding pipes with parallel horizontal steel pipes. The UDM had to be at minimum about 0.4 m and at maximum about 2.75 m from the nearest object to collect accurate data. As such, the boxes were placed as high as possible in anticipation of high tidal levels.

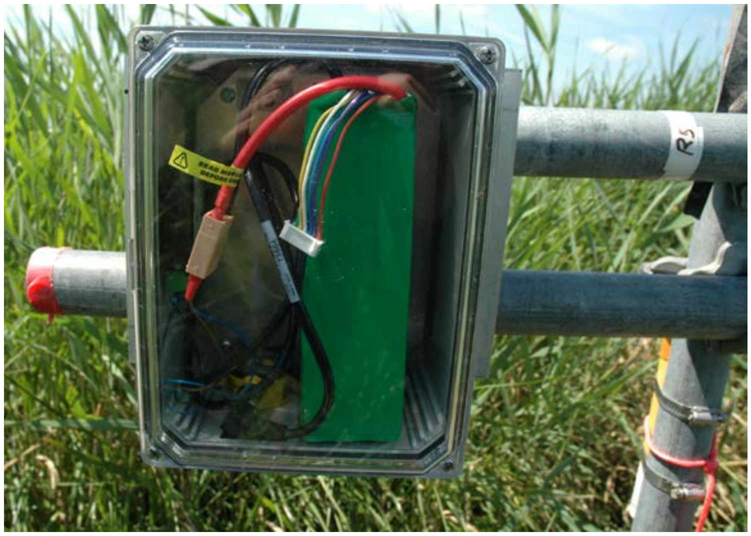

Figure 9: Example of box containing Madgetech Volt101A data logger, lithium p-polymer battery, and UDM.

The Vector current meter was attached to an aluminum cross-shaped mount on the bed at station R0 (Figure 10), placed such that the cabled three-pronged probe faced upward and correctly aligned with the horizontal instrument tube. The instrument tube was wrapped in electrical tape to protect it from biological growth throughout the study. The Vector measured velocities along three axes in a 0.015 m diameter sampling volume 0.15 m above the central transducer of the probe. The central transducer was 0.38 m above the bed. The transducer sends out acoustic pulses, and the resulting echo is received by the three receiver prongs. The time lag between pulses is used to find the Doppler shift, which is converted to water velocity using temperature measurements and the speed of sound in water.

Figure 10: Photograph of ADV on aluminum cross-shaped mount, from which the pressure sensor had been removed (taken by Evan Krape).

The ECM probes were positioned to face downward, such that one axis pointed directly offshore and the other pointed alongshore, with the centers of the probes positioned 0.1 m above the ground. They use a magnetic field to determine these velocities. They return noise when the probe is dry or the water depth does not completely contain the probe. The ECM compass required separation from steel components, so an aluminum pipe was used to hold the instrument. While stainless steel hose clamps were used to attach the instrument to the aluminum pipe, and steel clamps were used to attach the aluminum pipe to the frame, the probe was far enough away so as there should have been little to no effect on the compass.

At stations R1 through R3, the sensor diaphragms of the pressure gauges were placed directly on top of the wooden boards, facing downward. At station R0, the pressure gauge was oriented sideways to fit with the aluminum mount. The distances between the ground and the pressure diaphragm were recorded. All pressure gauge sensor diaphragms were protected with a covering of fine mesh. The sensors recorded pressure over time. The water depths were shallow enough such that the pressure gauges should have been able to effectively capture wave-induced pressure fluctuations.

A Brinno TLC200 PRO time lapse camera was set up on a steel pipe between the transect and the dock to take an image every 30 seconds (s) during daylight hours. This camera captured ship passages, ship wakes, tides, and any anomalies during the day (such as birds wandering around the transect) throughout the entire study.

Regular visits were made to the island to download data, clear instrument memory, and swap out batteries. The “intense” studies required more frequent visits. After the initial deployment and during each visit, dead and live vegetation around R4 and R5 were cleared away so as to give the UDM a clear path to the bed. During each visit, the distances between the UDMs and the bed, between the bottoms of the pressure gauges and the bed, and between the centers of the ECM probes and the bed were measured and noted. At R1, the distance between the central transducer of the Doppler current meter probe and the bed as well as the distance between the pressure gauge and the bed were recorded. These measurements were used in data processing and analysis. The time of day for each measurement and movement of the instruments were also recorded.

Elevation surveys along the transect were conducted regularly using a Leica real-time kinematic global positioning system (RTK GPS), referenced to the North American Vertical Datum 88 (NAVD88). These surveys were done to obtain cross-shore profiles along the transect and monitor morphological changes throughout the month. Survey data points were taken approximately every meter from as deep as the operators could go (usually 5 to 10 m offshore beyond station R0), at the locations of the data collection stations, and up to about 6 m onshore of station R5.

In the middle of the study on June 20, 2018, characteristics of vegetation along the transect were measured using a 1 m^2 polyvinyl chloride (PVC) quadrat. Four 1-m PVC pipes were connected into a square frame using four 90° PVC elbow connectors. The frame fit together such that each side measured 1 m. This quadrat was placed along the transect in the vegetation patch to estimate stem density. Only stems fully inside the 1 m^2 quadrat were counted. Calipers were used to measure stem diameters and leaf widths at the widest points. As *Schoenoplectus pungens* stems have triangular cross-sections, the stem cross-sectional size was measured as the length of a triangular side (Chatagnier, 2012). Tape measures were used to measure stem heights and leaf lengths. The *Schoenoplectus pungens* and the dry brown *Phragmites australis* had no leaves to measure. The measurements were averaged for each species.

Photographs and samples of the vegetation along the transect were taken to compare to Delaware wetland plant guides for species identification. There was a monotypic stand of *Schoenoplectus pungens* between R3 and R4 and a smaller monotypic stand of likely invasive *Phragmites australis* between R4 and R5. There were small amounts of moss and clover on the face of the peat terrace edge.

Shipping log data (MarineTraffic data) were obtained from the Maritime Exchange for the Delaware River and Bay, providing approximate information about when cargo ships passed through major port areas, their size, speed, and deadweight tonnage. When a ship appeared at multiple ports in the same day in the data log, the ship direction and time of passage by Pea Patch Island could be interpolated or extrapolated. This was useful for identifying cargo ships throughout the entire day. If a ship passage occurred during daylight hours, it could be cross-referenced with the time lapse camera imagery. The time lapse camera imagery was reviewed, and each ship passage and ship wake were recorded with corresponding ship type and direction.

However, the MarineTraffic data includes only registered cargo ships, which did not include every ship that passed the island. Sometimes multiple ships had similar timestamps at ports and were travelling in the same or opposite directions. Also, sometimes they were too far away for identification using time-lapse imagery.

2.3 Data Processing

The raw data had to be cleaned and processed before the data could be analyzed. Data collected during the last day of the study were removed from consideration because the pressure sensor at station R0 started giving erratic measurements, indicating a dying battery. The pressure data were adjusted using the measured atmospheric pressure data from the pressure sensor at station R5. First, the atmospheric pressure data were interpolated across the time vector of the other pressure sensors. The atmospheric pressure data fluctuated due to changes in weather and temperature, but stayed mostly the same around the average for Delaware. Water temperature data recorded by the ECMs and water salinity data recorded by nearby National Oceanic and Atmospheric Administration (NOAA) stations and confirmed using a conductivity meter were averaged and used to estimate water density. The water had a salinity value of about 1. Depth data were obtained by subtracting the atmospheric pressure data from the pressure data and dividing by the estimated density of water and acceleration due to gravity. If there was a measured distance between the bottom of the pressure sensor and the bed during portions of the study, that distance was added to the depth during that segment of the time series.

From the UDM data, water depths were obtained by subtracting the data from the measured height of the respective UDM during that time. Distances greater than 2.75 m or less than 0.40 m were removed, as these were outside of the measuring zone for the sensor. The depth data from R2 and R3 were compared with the depth data from the corresponding pressure gauges to ensure they approximately matched. While the sampling frequencies were different, the depth data obtained from the sensors indeed closely tracked each other. To obtain the water elevation from the UDM depth data, elevation data for each period of time were added to the water depth data.

Depth data were cleaned using a histogram of gradients across the data and setting an absolute value cutoff slope difference of 0.06, above which data points were removed. This method was used to reduce noise corresponding to unrealistic increases or decreases in water level.

Sometimes animals, especially Canadian geese, walked around the stations and interfered with UDM data. These animals also likely pushed the vegetation under the path of the UDM. In these cases, the emitted acoustic pulses hit the vegetation or animal and recorded the distance between the sensor and the obstacle, rather than the water or bed. The geese interference at stations R0 through R3 were handled with the cutoff slope method.

In an attempt to at least partially remedy this problem, the water depth data at station R3 and the approximate elevation differences between stations R3 and R4 and between stations R3 and R5 were combined to determine when the recorded distance measurements were unrealistic. Apparent water levels higher than the elevation difference between station R3 and station R4 or R5, on top of the water depth at station R3, were interpolated with the rest of the data. This was justified because when there was no vegetation swaying, the differences between the water levels at R3 and R4 was approximately equal to the bed elevation differences between R3 and R4. Data during times when the sensors were dry, or times when the depth data at station R3 were lower than the height of the peat platform, were removed.

The UDM data were interpolated to the corresponding time series in the pressure gauge data to make them comparable. The UDM data were then concatenated for the entire study, leaving short gaps where the sensors were removed for downloading data and swapping batteries.

The ECM burst data are difficult to analyze because of the gaps and spikes in the data near the times when the sensor probes were dry or the water surface lapped against the probe. As the water level wavers above and below the sensor probe limit, the probe cannot take accurate measurements. Those affected areas must be removed, but in doing so real data are also removed with it. This issue is combined with the burst mode measurements for the non-intensive parts of the study, and the fact that each sensor measured velocity at a single point. ECM data during times when the water level was below 0.15 m were removed, as it was observed there was excessive noise due to the water level not fully covering the probe. Velocity data with a slope difference above an absolute value of 0.02 were removed.

There are large tidal influences in the month-long data set (Figure 13), in addition to long-term fluctuations due to weather patterns. The time since deployment is displayed in days in Figure 13 to indicate overall tidal cycle patterns. The water depth drops to zero at low tide when water no longer reaches station R3. Removing the tidal influence from the data would reduce potential tidal effects on the analysis results and allow for wave parameter analyses. It is useful to consider the longer-term fluctuations in the data in an attempt to remove them. Fourteen tidal constituents (M2, S2, N2, K2, K1, O1, P1, Q1, S1, MF, MM, SSA, M4, and MS4) were used to process demeaned data, considering solar and lunar semidiurnal, solar and lunar diurnal, and some long-period effects. The tidal influence could not be completely removed in this way, but the overall range of depths in the dataset was reduced.

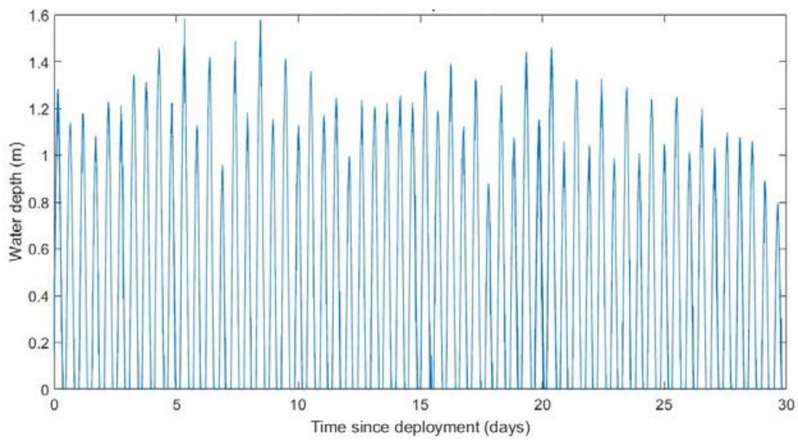

Figure 13: Unfiltered water depth at station R3 without removal of the tide.

After removing tide using semidiurnal, diurnal, and long period tidal constituents, there were still long-term periodic patterns in the data set (Figure 14). While this method may not be the best, it is important to gain a better understanding of why it may not work well to inform a better approach. The time since deployment in Figure 14 is shown in hours to show how some patterns change over the course of several hours. Using a lowpass filter indicated that these remaining oscillations varied in amplitude and period over time. Using a highpass filter allows one to attenuate these long-period oscillations, but an ideal threshold is difficult to determine. The long-period oscillations could be due to weather or perhaps a continuous time of high winds pushing water into the area near the site. Seiche, or standing waves in a body of water with solid boundaries, is not likely because the dock near the site allows a lot of water to go through. There may have been some reflection off of the dock pilings, but not likely enough to create consistent standing waves.

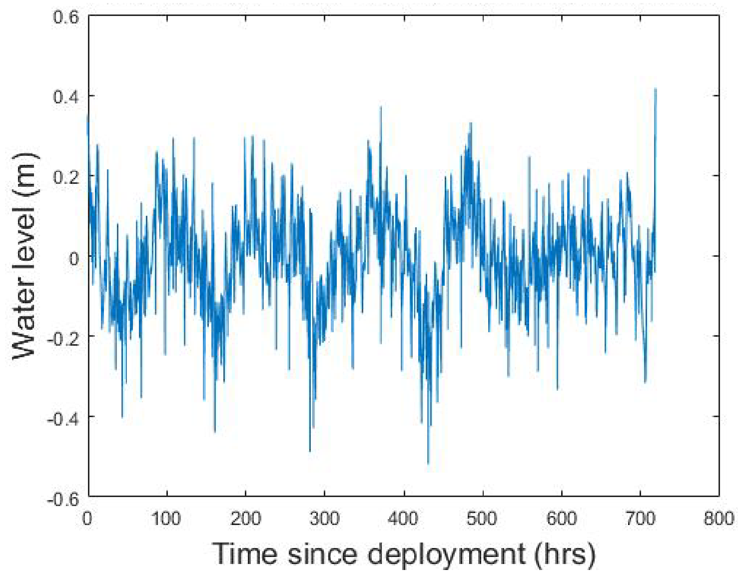

Figure 14: Tide-removed water level data at station R0 using the tide removal function involving 14 tidal constituents.

The results of a second-order lowpass filter and highpass filter with a cut-off period of 100,000 s (about 27.8 hours) are shown in Figure 15. The highpass filter, or essentially the subtraction of the lowpass filter results, should have attenuated shorter-term tidal and weather effects, but there are still long-term oscillations. The amplitude of these oscillations varies over time.

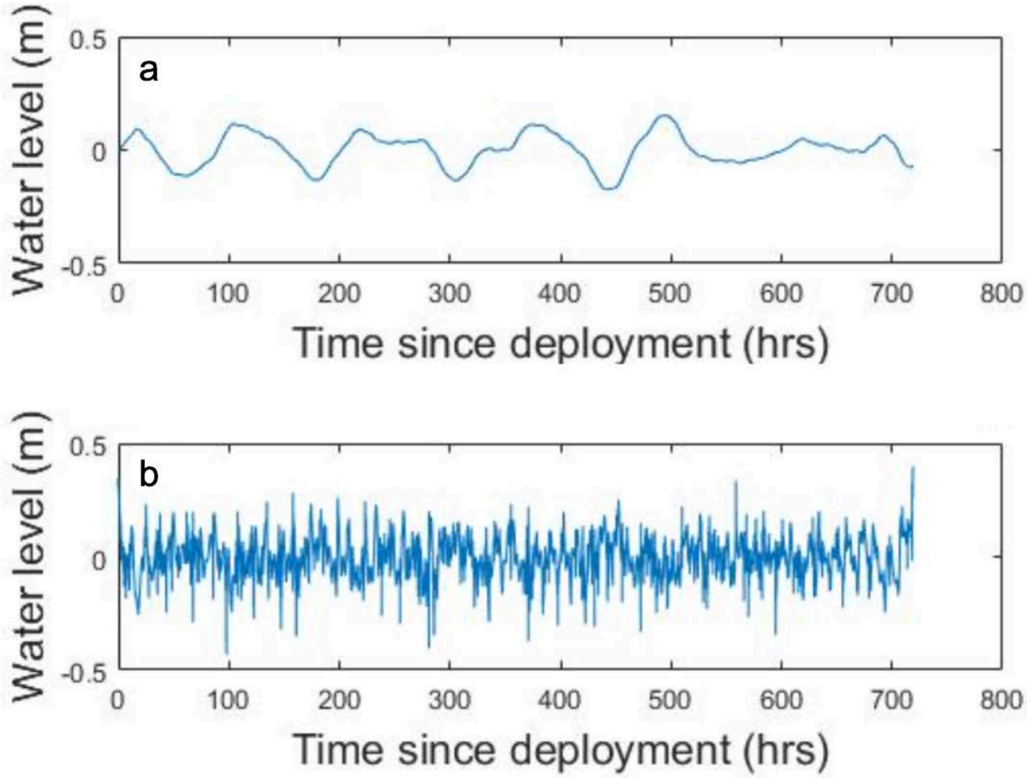

Figure 15: Water level data from station R0, from which tidal signals are removed using tidal constituents, passed through a) low pass and b) high pass filters using a cutoff period of 100,000 s.

In comparison, use of a second-order lowpass filter and a cut-off period of 10,000 s (about 2.8 hours) results in the same lowest-frequency oscillations with the addition of oscillations with a period between 10,000 s and 100,000 s (Figure 16). The corresponding highpass filter is an improvement over that of the 100,000 s period highpass filter, but still has smaller long-term oscillations. Decreasing the threshold below 1-hour decreases these oscillations, but they still exist.

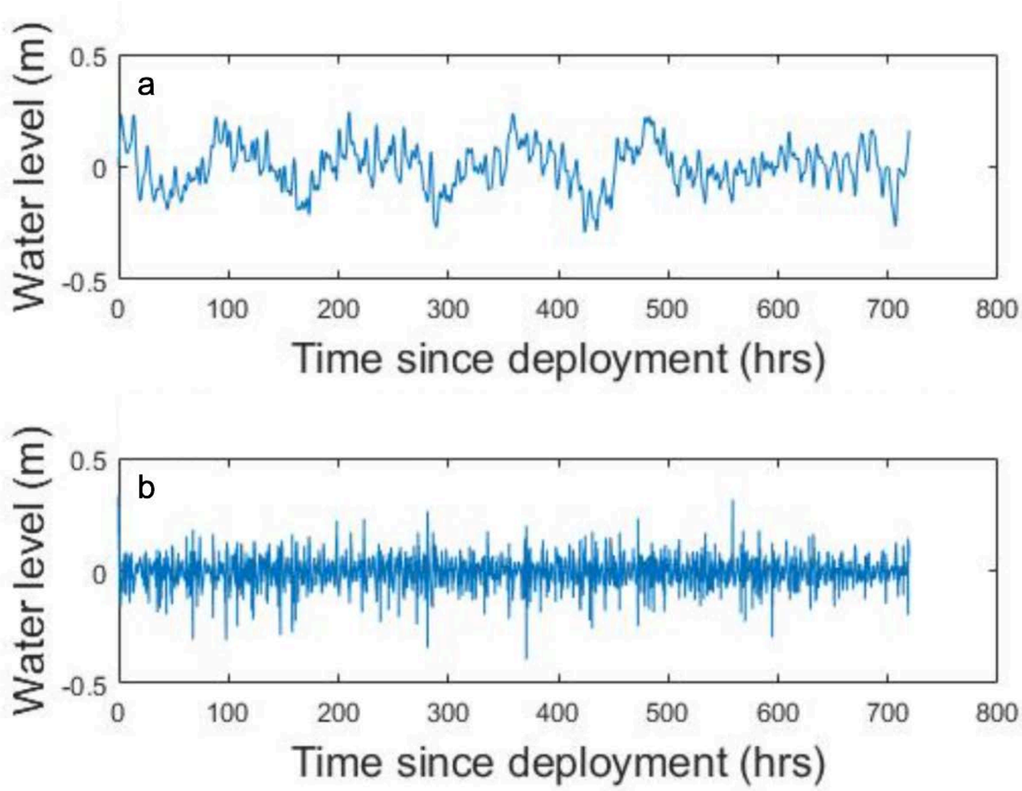

Figure 16: Water level data from station R0, from which tidal signals are removed using tidal constituents, passed through a) low pass and b) high pass filters using a cutoff period of 10,000 s.

Another alternative, ultimately chosen, involves subtracting a moving average from the low-frequency data, without the use of tidal constituents. Using a window of 900 s (15 min) multiplied by the sampling frequency, 16 Hz, results in the signal in Figure 17. Over the entire time period, the results appear similar to that in Figure 16, but some of the higher spikes appear to have been filtered out by the corresponding high pass filter. Zooming in shows that long-period oscillations have been essentially removed. Decreasing the period threshold for a lowpass and highpass filter could attenuate more of these periodic fluctuations, but using a moving average appears to give more useful results. The moving average itself was kept as the approximate tidal record to use later as mean water level data.

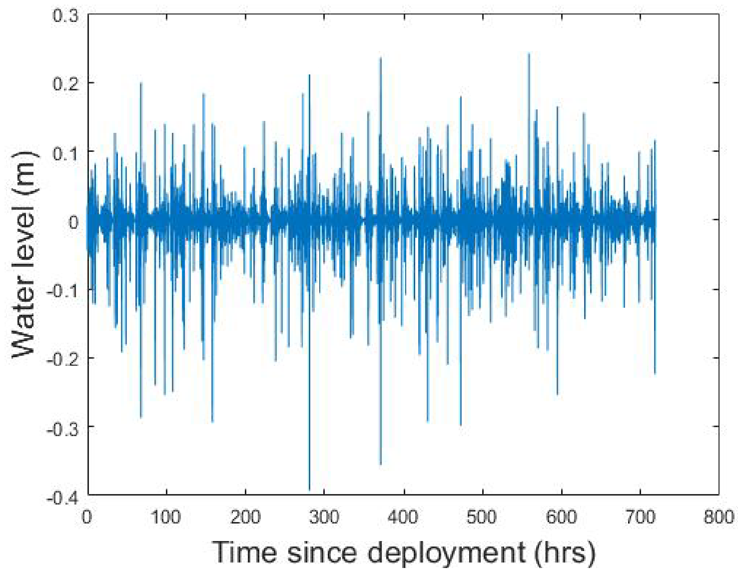

Figure 17: Tide-removed water level data at station R0 using a subtraction of a moving average, without the use of tidal constituents.

2.4 Data Analysis

Ship wakes can be detected fairly easily by eye by looking for dense spikes in the time series, but going through a month-long data set manually is tedious and prone to human error. There are multiple ways to automatically flag potential ship wakes. However, no method is perfect, as ship wakes are inherently different, depending on ship direction, size, weight, speed, and local tides.

One option, which was ultimately chosen, is to use a function to automatically detect peaks in the data, with parameters for the minimum peak height and minimum distance between peaks. The MATLAB “findpeaks” function was used for this purpose. The function is flexible and allows for input arguments such as a minimum peak height and minimum distance between peaks. Setting the minimum peak height threshold too high still catches wakes from cargo ships passing close to the island wakes but misses wakes from cargo ships passing far away from Pea Patch Island, the Delafort ferry, and other small boats. Ship-generated waves, especially during low tides, did not reach all of the data collection stations. Stations R4 and R5 were affected by ship wakes only during higher tides when the water level rose above the peat platform. At the same time, setting the minimum peak height threshold too low would double count some larger ship wakes. Often two ships would pass the site at the same time, generating overlapping and intersecting ship wakes, making it difficult to automatically differentiate how many actual ship wakes occurred. Other times during relatively low wind conditions, sudden increases in wind speeds could cause a signal that resembles a wake generated by a smaller ship. This signal could be identified by the function as an actual ship wake.

Another method that was tested is to use cross-correlation of a typical ship wake against a longer time series. This algorithm involves large matrices and is inefficient and time-consuming. Using one typical ship wake may lead to poor correlation with a differently structured ship wake. One must determine a correlation coefficient threshold to decide what is counted as a ship wake and what is not.

A ship wake was chosen from the water depth time series at station R0 (Figure 18). The ship wake time series itself was cross-correlated against a wider time series including the ship wake. As expected, the correlation coefficient at the start of the ship wake event rose sharply to 1. The rest of the time series had correlation coefficients of no more than around 0.4.

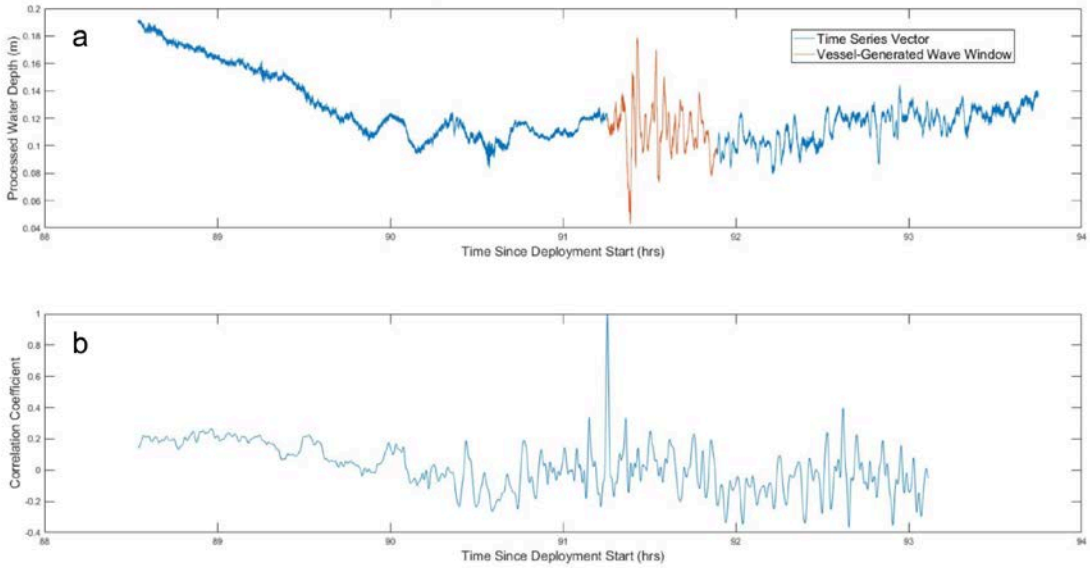

Figure 18: a) Water depth time series containing highlighted ship wake window; b) Cross-correlation coefficient of test ship wake from a) across time series from a).

The method does not work well with ship wakes that do not have highly defined drawdowns and surges. While such ship wakes have elevated water levels relative to wind waves, the shape does not contrast as well. Note that this method was attempted in conjunction with using tidal constituents to remove the tidal influence. Removing the moving average likely would have improved the accuracy of this correlation method, but does not change the fact that the method is highly inefficient and can essentially only be used on small segments of data at a time.

An additional method is to use the first or second derivative to find the highest instantaneous changes in the data. One issue with this is some ship wakes have larger drawdown and uprush than others, such that some register as large spikes in the derivative plots while others don’t even register as blips. The data could be passed through a heavy low pass filter to try to isolate ship wakes before first or second derivatives are computed, but this filter would have to be carefully done to avoid filtering out parts of ship wake chirp signals. The smaller ship wakes and wakes with lower drawdown and surges could still be passed over.

Another possibility is to analyze spectrograms, or windowed Fourier transforms (Herbert et al., 2018). The main idea is that the higher power density of ship wakes would stand out against the power density of normal ambient wave action. The spectrogram would need to be accurately tuned and some form of power spectral density threshold algorithm would still need to be used to automatically identify ship wakes from spectrograms. In the presence of ambient wind wave action along the Delaware River, spectrograms are more difficult to use.

The function of automatically finding peaks is not perfect and will not be able to automatically identify all ship wakes with complete accuracy, but is more efficient and accurate than the other described options. Setting a higher minimum peak height threshold could help find more impactful and influential ship wakes that could have a higher erosive effect on the shore. While the frequent passage of the Delafort ferry may be an interesting topic of study and indicate erosional effects, they may be minimal relative to those induced by larger cargo ships. In any case, this function was used to separate out two groups of ship wakes. The group with the higher threshold is expected to include primarily wakes from cargo ships passing closer to the island. The group with the lower threshold is expected to consist of wakes from cargo ships passing farther away from the island, ferry boats, and other smaller boats. It is possible stronger wind events registered in one of these groups. Some wakes from smaller ships may not have been caught by the lower threshold, but lowering the threshold any further could capture more wind events. The minimum peak threshold for large ship wakes (and maximum peak, exclusive, for small ship wakes) was 0.0325 m and the minimum peak threshold for small ship wakes was 0.0165 m.

The identified peaks at station R0 were used to separate out and isolate ship wake events. Each ship wake is different, lasting for different amounts of time with varying structures. For the larger ship wakes, the event was extended to the last peak before the drawdown to 15 min after the location of the associated peak. For the smaller ship wakes, the event was extended 10 s before the associated peak to 10 min after the associated peak. The purpose of doing so was to make the ship wake time windows uniform for comparison. This method and the thresholds numbers were improved through trial and error.

Each identified ship wake was carefully considered. If it did not look like a ship wake, if there was an odd blip in the data that caused it to be identified, or if it looked like two ship wakes occurred at once, the wake was removed. The peak method used at station R0 found 207 larger ship wakes and 245 smaller ship wakes. Twelve larger ship wakes and 21 smaller ship wakes were removed, leaving 195 larger ship wakes and 224 smaller ship wakes. The kept and removed larger and smaller ship wakes are shown in Chapter 3.5.

Ship wakes at stations R1 through R5 were identified by finding the water level data recorded during slightly forward shifted time windows corresponding to the time windows for the kept ship wakes at station R0. This way, the ship wakes detected at station R0 could be tracked across the transect. Sometimes the water did not reach stations R2 through R5. During lower tides when the water level was below the peat platform elevation, the ship wakes would not reach stations R4 and R5.

As such, it is useful to divide the comparisons and further analyses into multiple categories: the entire transect, the unvegetated section from R0 through R3, the vegetated section from R4 to R5, and the peat platform edge between R3 and R4.

For the purpose of this categorization, two more groups of ship wakes were created: one in which ship wakes that did not affect station R3 were removed, and another in which ship wakes that did not affect station R5 were removed. This was done to give a higher sample of ship wakes to use in comparing stations R0 through R3, as stations R4 and R5 were affected by a more limited number of ship wakes.

Individual wave heights and periods in large ship wakes were estimated using the zero down- crossing method on demeaned tide-removed data (Figure 19). The main concept behind the method is that zero represents the average water level at the location of the sensor, and fluctuations above or below zero represents pressure fluctuations and thus wave action. These methods involve locating the times where the depth data goes down or up across zero, respectively, and takes the difference between the maximum and minimum recorded depth between consecutive zero down-crossings as the height of that wave. The time between consecutive zero crossings was taken to be the period of that wave.

There are waves of different frequencies travelling together, superimposed on each other, so this method does not perfectly describe the waves. Sometimes smaller ripples appeared in the record as slightly above zero, but not crossing it. This resulted in small wave heights and long periods for those segments. These were removed from the wave height and period calculations using cut-offs for low- (410 s) and high-frequency (7.5 s) waves. These cutoffs were decided by examining the low-frequency and high-frequency components of ship wakes and ambient wind wave conditions, and determining the highest wave periods within realistic low-frequency and high-frequency ship wakes. These cutoffs were also used, in addition to filtering, to remove any remaining drawdown and surge influence when considering high-frequency waves, so that it would not be counted twice. For small ship wakes, the zero down-crossing method was used when the initial data point was above zero, while the zero up-crossing method was used when the initial data point was below zero. High-frequency components were separated from low-frequency components using a moving average with a 75-s window.

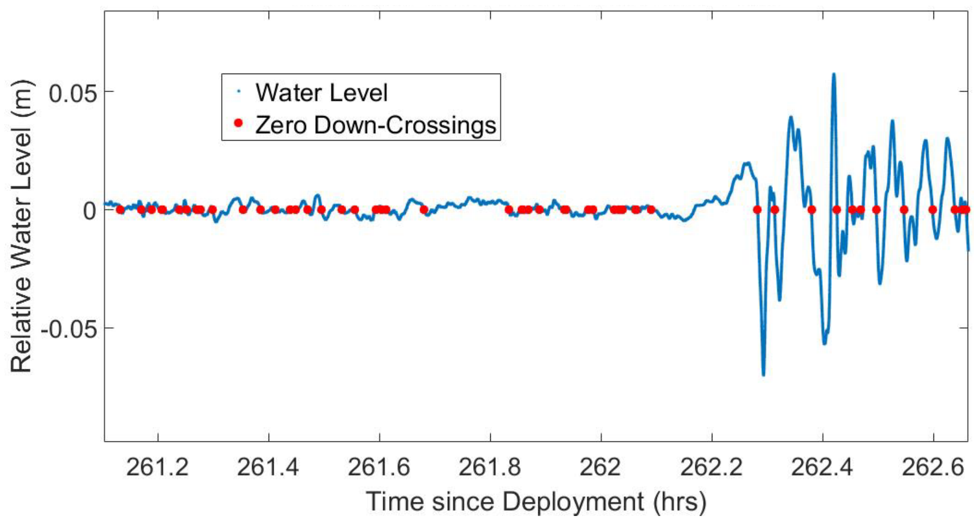

Figure 19: Example of applying the zero down-crossing method to data at station R0, and the limitations of the method.

As the data set stretches over a month, the statistical parameters such as the mean and standard deviation cannot reasonably be assumed constant over time. This is due to changing weather and atmospheric patterns, and can be seen in the aforementioned problems with trying to remove the tidal influence using tidal constituents. As such, statistical wave parameters must be estimated from smaller segments of the data so that these smaller segments can be assumed stationary. Ship wake windows (10-15 min) are short enough for such calculations.

Wave energy can be estimated in the time and frequency domains. In the time domain, using small-amplitude linear wave theory, wave energy density per unit surface area (Joules per square meter) can be described as (Kamphuis, 2010):

$$E = \frac{1}{8}\rho g H^2, \tag{8}$$

where H is the wave height. The energy density is proportional to the wave height squared, indicating a higher energy density for a greater wave height and a smaller energy density for a wave height below 1 m. Wave power, or wave energy flux, per unit wave crest length (Watts per meter) is defined as the energy density per unit surface area multiplied by the group velocity C_g, the speed at which wave energy moves (Kamphuis, 2010):

$$P = EC_g. \tag{9}$$

The wave group velocity can be found as follows (Kamphuis, 2010):

$$C_g = nC, \tag{10}$$

where n is the group velocity parameter and C is the wave phase speed. The group velocity parameter can be calculated as (Kamphuis, 2010):

$$n = \frac{1}{2}\left(1 + \frac{2kh}{\sinh(2kh)}\right), \tag{11}$$

where h is the water depth and k is the wave number. The wave number is (Kamphuis, 2010):

$$k = \frac{2\pi}{L}. \tag{12}$$

where L is the wavelength. The phase speed can be found as (Kamphuis, 2010):

$$C = \frac{L}{T}, \tag{13}$$

where T is the wave period. The following equation for wavelength L was iterated until convergence (Kamphuis, 2010):

$$L = \frac{gT^2}{2\pi}\tanh(kh). \tag{14}$$

The energy densities and fluxes calculated for the wave heights and periods in each ship wake can be summed, averaged, and compared to each other.

Wind wave energy can be analyzed by summing up energy densities and fluxes of wind waves in short segments of time, as wind conditions change throughout the day. There was a buoy located near Delaware City that collected wave height data, but the data recorded from that buoy was not recording during the field experiment. Thus, wind wave conditions were estimated by first removing the found ship wake windows from the data. The wind wave energy across those ship wake windows was later roughly estimated by using average wind wave heights before and after the ship wake windows, and interpolated across the windows.

Removing background wind waves from ship wakes allows for better comparison of wind waves and ship wake energy. Hofmann et al. (2008) used a wave period threshold of 0.4 Hz (2.5 s) to differentiate wind waves from ship wakes on Lake Constance. Gharbi et al. (2008) used a wave period cutoff of about 0.6-0.7 Hz (1.4 to 1.7 s) to distinguish between wind waves and ship wakes on the St. Lawrence River. Larger ship wakes have longer wave periods than smaller ship wakes, making it more difficult to determine to fine line in wave period between small ship wakes and wind waves. A cutoff of 1.75 s was chosen based on power spectral density curves from the demeaned water level data, and examination of the actual high-frequency periods of the ship wakes. Wave periods below 1.75 s were removed from consideration in estimating ship wake energy.

Use of anemometers to measure wind speeds throughout the day could have helped provide additional estimations or validations through consideration of wind fetch and duration. Anemometers could have also provided information on wind directions.

One could divide the wave height reduction between R4 and R5 by the distance between them and represent that as the wave height reduction per meter. This may not be accurate because, as mentioned before, most of the wave height attenuation occurs at the seaward edge of the vegetation patch (Knutson et al., 1982). Such a division could overestimate the attenuation caused by vegetation farther landward into the patch, and in so doing underestimate the attenuation caused by vegetation closer to the leading edge of the patch. As such, it would be more useful to consider the attenuation between stations R4 and R5 without further divisions.

Chapter 3

RESULTS AND DISCUSSION

3.1 Cross-shore Profile Data

The Leica RTK GPS survey cross-shore distance and elevation data were plotted to construct a cross-shore transect profile (Figure 20). Each color represents a different survey. The black dots represent each station along the transect. A survey was attempted during every visit, but sometimes surveying was not done due to high tide levels.

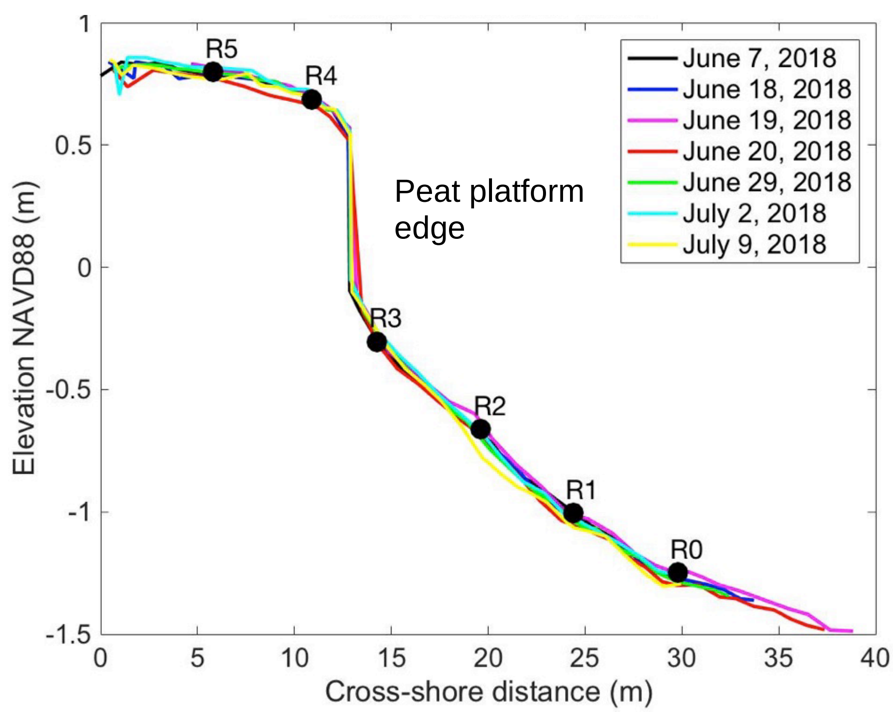

Figure 20: Leica RTK GPS transect elevation cross-shore profile survey data.

The peat terrace edge is represented by the vertical line sections in the plot, and is about 1 m in height. The slope of the ground in the vegetation patch on the peat terrace is gentler at approximately -0.02 (-2%). The slope of the ground offshore of the peat terrace between stations R0 and R3 is steeper at roughly -0.06 (-6%). The distance between R0 and R5 is about 24 m.

The seven survey data sets do not line up exactly on top of one another. One possible reason is slight morphological changes over the course of the month due to sediment transport. Another potential cause is different people conducting the survey, as different people may let the bottom of the surveying rod just touch the top of the ground or let it slightly sink into the ground. There may have been some alongshore variation around the stations.

3.2 Vegetation Characteristics

The average vegetation characteristics estimated from measurements taken on June 20, 2018 are presented in Table 1. The *Phragmites australis* along the transect (Figure 21a) appeared to be grouped into roughly three different growth stages (Figure 22). The oldest, the tallest plants that were browning and drying out, represented the largest measurements (although there were a small number of tall green individuals). The shortest plants, many without seedheads or with seedheads just starting to grow, represented the smallest measurements. During the April 20, 2018 visit, the entire vegetation stand was yellow-brown and had fully matured seedheads (Figure 6), pointing to the death of most of the stand and a subsequent growth period in May. Buds and shoots were also observed in the area offshore of the peat terrace along the transect, but these did not grow. It is possible those plants were eaten or cleared.

Similarly, the *Schoenoplectus pungens* along the transect (Figure 21b) consisted of roughly three different growth stages. *Schoenoplectus pungens* were not noticed during the April 20, 2018 visit. The tallest plants started developing seedheads first. Throughout the course of the study, the younger plants grew and matured. Ideally vegetation measurements would have been taken at least at the beginning, middle, and end of the experiment to observe changes.

Figure 21: a) *Phragmites australis* along study transect; b) *Schoenoplectus pungens* along study transect.

Figure 22: Photograph of range of *Phragmites australis* ages and stem heights within vegetation patch.

Average characteristics	*Phragmites australis*	*Schoenoplectus pungens*
Density (m^{-2})	620	9200
Stem height (cm)	Short: 116 Medium: 138 Tall: 174	Short: 55 Medium: 67 Tall: 83
Stem diameter (mm)	Short: 2.5 Medium: 4 Tall: 5	Short: 1 Medium: 1.5 Tall: 2
Leaf length (mm)	Short: 280 Medium: 350 Tall: 500	No leaves
Leaf width (mm)	Short: 10 Medium: 20 Tall: 45	No leaves

Table 1: Average vegetation characteristics along transect.

Note the extreme difference between density estimations in Table 1. The patch of *Schoenoplectus pungens* was so dense, the stems could not be individually counted. Multiple counts were made of stems along each 1-m side of the quadrat, and the density was estimated considering the uniform distribution of stems. While at first sight the *Phragmites australis* patch may appear denser than the *Schoenoplectus pungens* patch, the *Schoenoplectus pungens* stems were much thinner than those of *Phragmites australis*. There were small patches of moss and clover on the face of the peat platform edge, but these were too flat and sparse to protrude outward from the face and cause appreciable flow disturbances.

An individual *Phragmites australis* plant may in itself provide more frontal volume blockage and attenuation of wave energy than a *Schoenoplectus pungens* plant, but the collective attenuation induced by the shorter and thinner but denser plants may be comparable or greater than that induced by the taller and thicker plants. The leaf dimensions for the *Phragmites australis* are not especially impactful on wave attenuation, as most high-tide water levels were mostly below common points of leaf development on the stems.

It must be noted that water entering the *Phragmites australis* patch already passed through the *Schoenoplectus pungens* patch and thus has less energy, which could affect the relative attenuation between the two species. The relative attenuation is difficult to estimate because of the presence of the peat platform edge between station R3 and the elevated vegetation patch.

Taking the average medium stem width to represent average overall stem width, and the average stem density per m^2, the frontal area per unit volume for *Phragmites australis* is approximately 2.48 m^2 per m^3. The frontal area per unit volume for *Schoenoplectus pungens* is approximately 13.8 m^2 per m^3. The vertical profile of the frontal area per unit volume for both vegetation species would likely be near constant for the expected water levels at stations R4 and R5. If the water levels frequently reached the height of the branching *Phragmites australis* leaves, the frontal area per unit volume would increase with distance from the ground.

3.3 Water Depths during a Ship Wake Event

Example water depth data at stations R3, R4, and R5 during a ship wake event are shown in Figure 23. The top image shows a time lapse camera snapshot of the event with a box around the responsible ship. The event occurred on June 12 at about 11:18 AM during high tide, so the ship wake is less visible than at low tide. R0 and R1 are completely submerged at this time. The panels on the left show the ship wake event in the context of a longer time series, while the panels on the right correspond to the black boxes in the panels on the left. The top, middle, and bottom rows correspond to stations R3, R4, and R5. The x-axis represents the time since deployment. The y-axis ranges are not the same for all panels and stations due to the presence of the peat platform, and to best show the features of the data. Dots were used to better show the differences in the structure of the ship wake between stations R3 and R4.

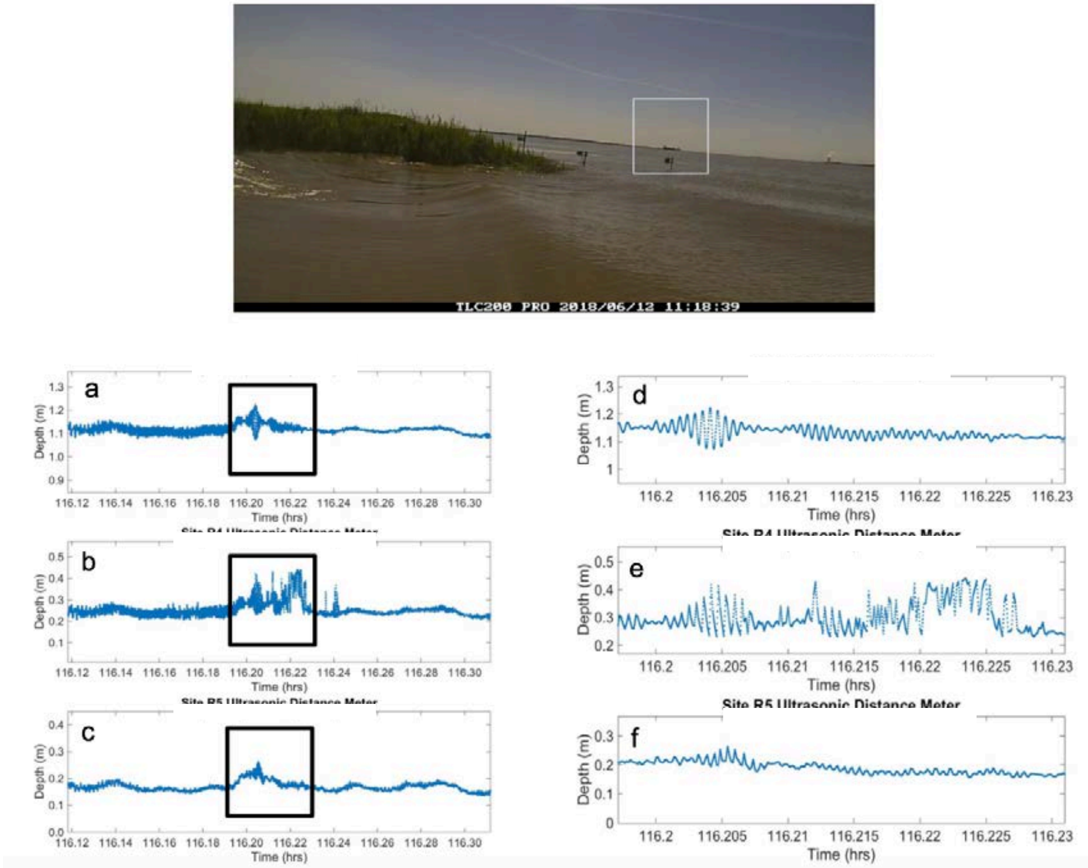

Figure 23: Example water depth data across vegetation patch during ship wake event: a) Station R3; b) Station R4; c) Station R5; d) Close-up of Station R3 data from a); e) Close-up of Station R4 data from b); f) Close-up of Station R5 data from c).

Perhaps because the cargo ship is far away and not as heavily loaded as other ships, there is no distinct initial drawdown and surge seen in the data in Figure 23. Such a wake may be identified in the “smaller ships” category; the ship is larger than ferries and speedboats, but due to wave energy spreading may not have as much of an impact as closer or larger cargo ships. Water depths decrease between stations R4 and R5, indicating wave height attenuation.

The smooth periodic pattern seen in the top right panel in Figure 23 differs from the more jagged periodic pattern in the top middle panel. The peaks, representing individual waves, are sharper, and the increases in elevation appear faster than the decreases in elevation for each peak. This could be because waves are steep enough to break at or before station R4. The sudden decrease in water depth atop the peat platform likely contributes to the wave steepening and breaking. Perhaps a higher sampling frequency than 16 Hz could have yielded higher resolution data; the increases in water level appear to be faster than the decreases due to the differences in number of samples on either side of each peak.

The middle panel on the right side in Figure 23, showing data at station R4, features a long series of disturbances lasting for one to 2 min following the ship wake event. There are some continuing disturbances following the ship wake at R3, but not to the same degree. There are no such disturbances evident at R5. The continued disturbances after the initial wave group impacts could be due to wave energy reflection off of nearby peat terrace formations back into the vicinity of R4. Splashing at the peat terrace edge between R3 and R4 and potential swaying of vegetation due to wave impact could have also contributed. The data look real, so interference by swaying vegetation is not likely. Reflection is likely even more probable due to the diagonal direction of the ship wakes from the ship travelling far away at an oblique angle to the study transect. Trailing divergent and transverse wave trains arc off at different angles as the ship turns, and wave energy spreads over the length of travel. Perhaps the reflection is so heavily attenuated by *Phragmites australis* that the disturbances are not seen in the R5 data.

The vegetation aspect of the study is cruder than most laboratory studies focusing on vegetation-induced wave attenuation, where measurements can be made on small length scales and slope can be controlled. This study provides an aggregate view of wave attenuation through a large portion of the entire vegetation patch. Laboratory studies may use a smooth bed or sediment-covered bed, which could be fixed or moving. This field study was constrained to the natural slopes at the site. As mentioned before, a control transect would ideally be constructed on an adjacent unvegetated area with an initial slope of about 6% followed by a slope of about 2%, to better determine the wave height reduction that can be reasonably attributed to vegetation as opposed to gravity. However, such a transect would not be a true control, as the transect of interest includes a peat platform that affects the hydrodynamics of water entering the vegetation.

The peat platform edge immediately after R3 in the transect complicates the data analysis. It presents a hard obstacle to the flow field. When the water depth is below the height of the platform, waves hit the edge and reflect. When the water depth is above the height of the platform, some water will be held back or slowed by the platform edge while some will continue flowing over the top. This disrupts wave heights and flow fields, likely leading to turbulent boundary layers. Without the presence of the peat platform edge, it is likely there would be wave attenuation between R3 and R4 and the wave attenuation of *Phragmites australis* and *Schoenoplectus pungens* could be more easily compared.

The unvegetated segment of the transect is about three times steeper than the vegetated segment of the transect. Such a contrast brings up a potentially interesting problem in comparing the attenuation of wave height along the steep unvegetated part due to gravity and bed shear stress to the attenuation of wave height along the gently sloping vegetated part. As mentioned before, in vegetation patches bed-induced drag is negligible compared to vegetation-induced drag. The gravitational force due to the slight slope could have an added impact on wave attenuation, as waves are pulled back down. For example, the reduction in water depth changes shown in the bottom right panel in Figure 23 cannot necessarily be fully attributable to the *Phragmites australis* between stations R4 and R5.

3.4 Water Velocities during a Ship Wake Event

Example velocity data during a different ship wake event are shown in Figure 24. The top two images show the conditions before and during the ship wake, with the responsible ship outlined with a white box.

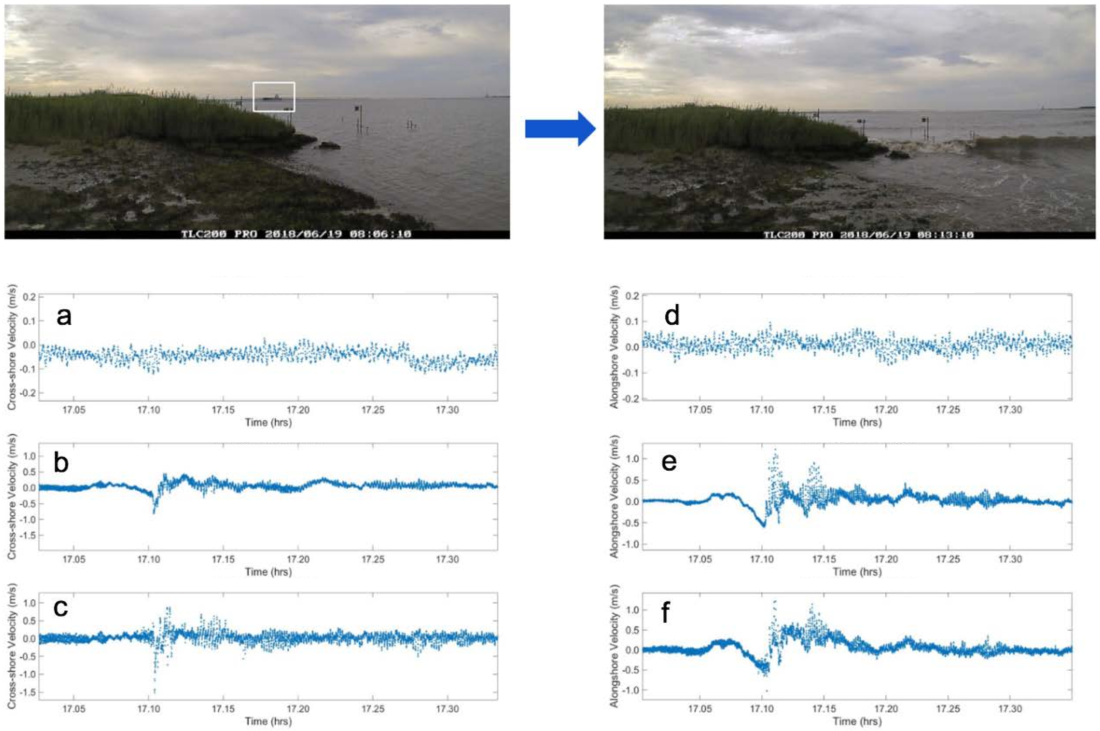

Figure 24: Example of water velocity data before and after a ship wake event: a) Station R3; b) Station R4; c) Station R5; d) Close-up of Station R3 data from a); e) Close-up of Station R4 data from b); f) Close-up of Station R5 data from c).

The event shown in Figure 24 occurred near low tide, making the wave crests of the ship wake more obvious in the time lapse camera image. The left three subplots consist of cross-shore velocity data at stations R0, R1, and R2, while the right three subplots consist of alongshore velocity data at stations R0, R1, and R2. The velocities recorded by the Doppler current meter at R0 were much lower than the velocities recorded by the ECMs. One possible reason for this is deeper water due to the steep slope relative to the other stations. The low tide could have affected how the sensor recorded data; the water level could have been within or close to the 0.15 m instrument blanking distance.

The water velocity responses to the ship wake at stations R1, R2, and R3 are consistent. There is an increase in onshore velocity as the ship wake begins to hit the shoreline, followed by an increase in velocity in the opposite direction as waves wash away. Both reach magnitudes of about 0.50 to 0.75 m/s. This is followed by continued dips of decreasing magnitude as time goes on. Turbulence around the sensor probe may affect the measured direction. This pattern applies for both cross-shore and alongshore velocities, likely because of the local angle of approach of the ship wakes relative to the shoreline orientation at the transect. The cross-shore velocity data at R2 do not have as defined a structure for the initial start of the ship wake as the other data. Velocity magnitudes reach 1.5 m/s at the initial increase in offs. Outside the ship wake event, velocities generally hover around 0.1 to 0.2 m/s or less.

3.5 Ship Wake Identification

The locations of the identified large ship wake peaks and small ship wake peaks are plotted on top of the overall water level data set for station R0. As mentioned before, initially 245 smaller ship wake peaks and 207 larger ship wake peaks were detected (Figure 25). After examining the ship wakes and removing ship wakes that did not resemble ship wakes or clearly appeared to be multiple ship wakes in quick succession (12 larger ship wakes and 21 smaller ship wakes) 195 larger ship wakes and 224 smaller ship wakes were kept for analysis. According to the shipping log, it is estimated that 397 cargo ships tracked by the system went by the island during the study period. Of those, 198 were travelling north and 197 were travelling south. Some of these may have been categorized as “smaller,” more likely some of the ships that passed on the east side of the island.

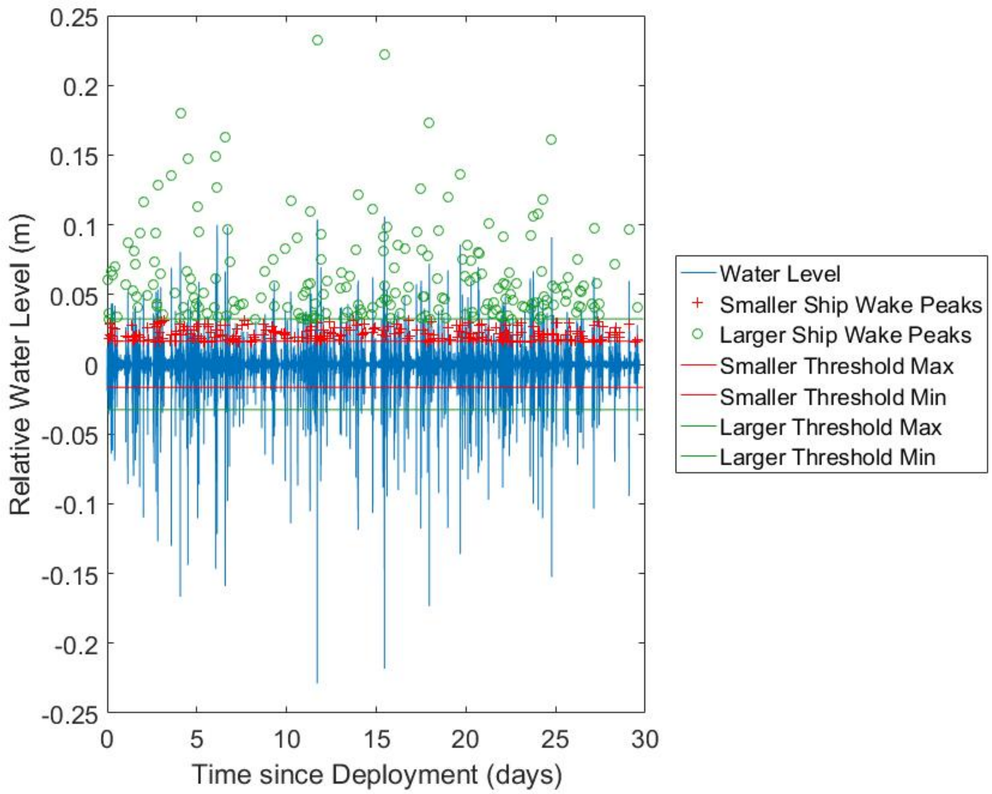

Figure 25: Automatically identified peaks from data at station R0, separated into larger and smaller ship wake categories.

The kept and removed low-frequency components of the larger ship wakes were plotted on top of each other to compare their shapes (Figure 26). The removed ship wakes show similar characteristics in that they include multiple ship wakes. The kept and removed low-frequency components of the smaller ship wakes were also plotted over each other (Figure 27).

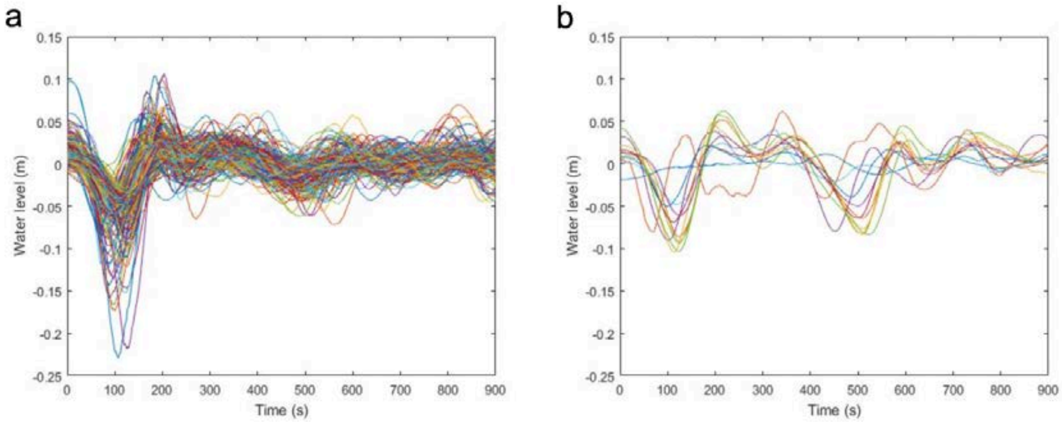

Figure 26: a) Low-frequency components of 195 kept larger ship wakes at station R0; b) Low-frequency components of 12 removed larger ship wakes at station R0.

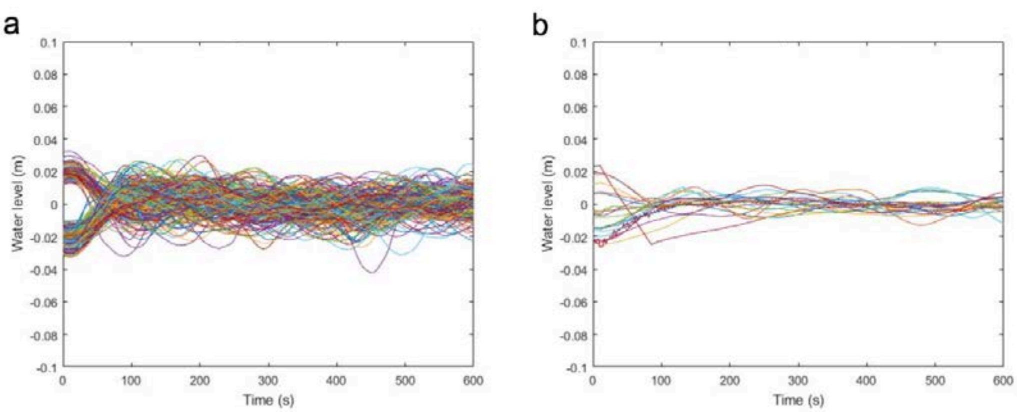

Figure 27: a) Low-frequency components of 224 kept smaller ship wakes at station R0; b) Low-frequency components of 21 removed smaller ship wakes at station R0.

The kept ship wake time windows at station R0 were applied to the data from stations R1 through R5, extended forward slightly to account for the time it would take water to travel between stations.

The 93 kept larger and 130 kept smaller ship wakes for stations R0 through R3 are plotted in Figure 28. The 19 kept larger and 30 kept smaller ship wakes for stations R0 through R5 are plotted in Figure 29. These are fractions of the 195 kept larger ship wakes and 224 kept smaller ship wakes found at station R0. One hundred two of the 195 larger ship wakes and 94 of the 224 smaller ship wakes did not reach Station R3. One hundred seventy-six of the 195 larger ship wakes and 194 of the 224 smaller ship wakes did not reach Station R5.

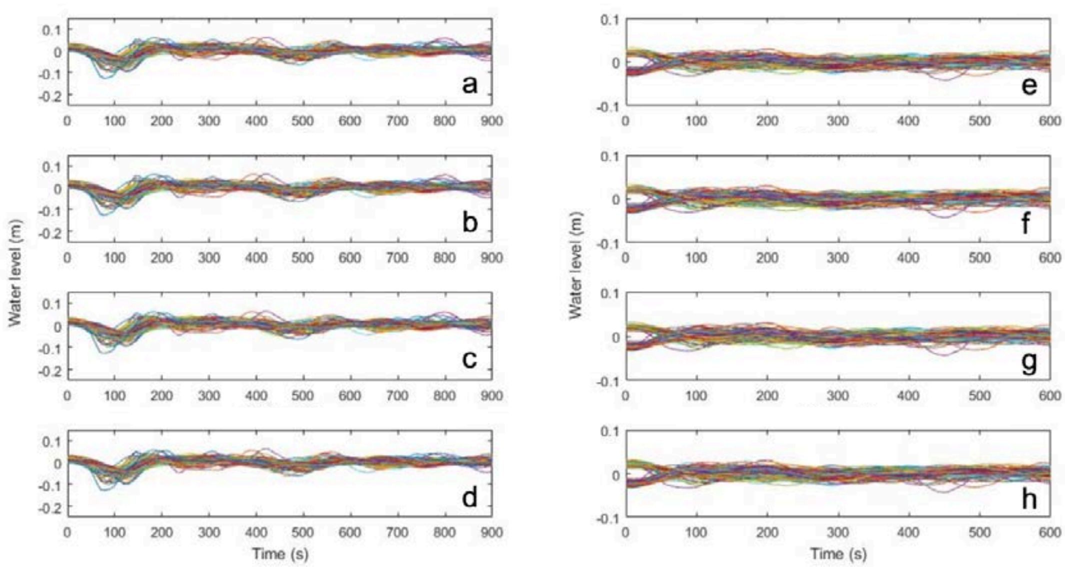

Figure 28: Low-frequency components of 93 kept larger ship wakes tracked through Station R3 at a) Station R0; b) Station R1; c) Station R2; d) Station R3; and 130 kept smaller ship wakes tracked through Station R3 at e) Station R0; f) Station R1; g) Station R2; h) Station R3.

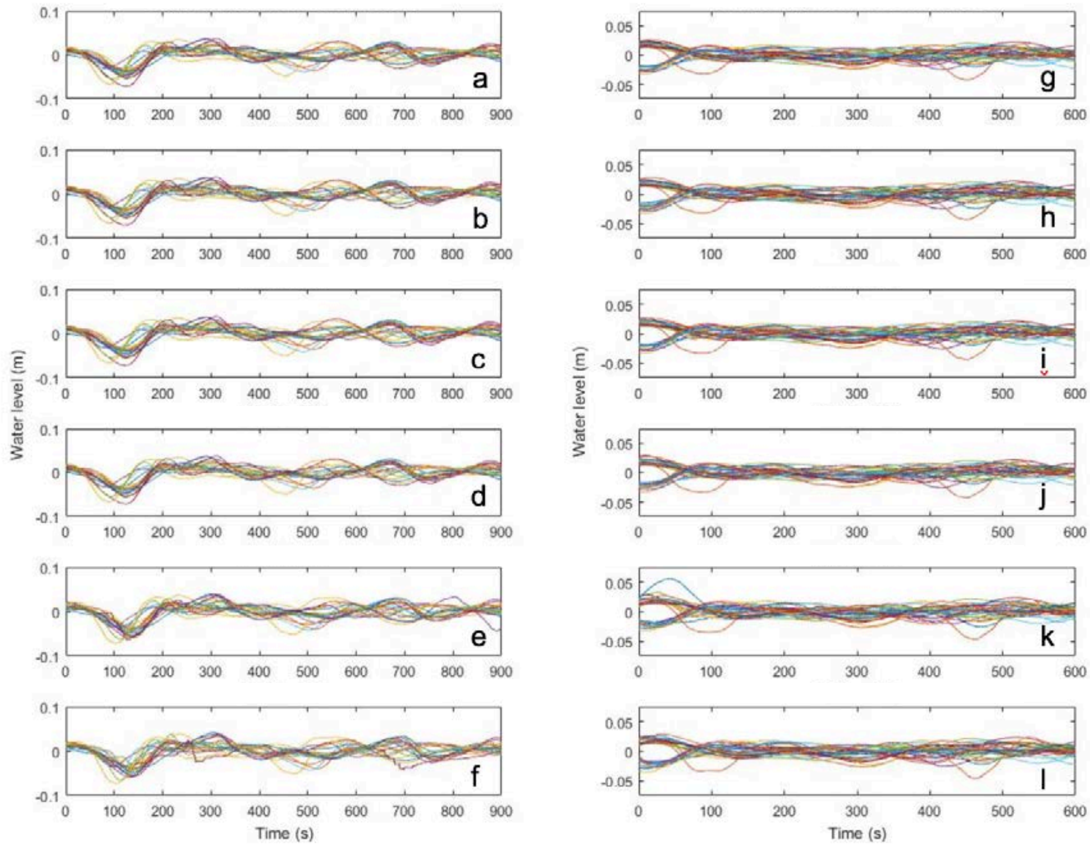

Figure 29: Low-frequency components of 19 kept larger ship wakes tracked across the entire transect at a) Station R0; b) Station R1; c) Station R2; d) Station R3; e) Station R4; f) Station R5; and 30 kept smaller ship wakes tracked across the entire transect at g) Station R0; h) Station R1; i) Station R2; j) Station R3; k) Station R4; l) Station R5.

The larger ship wakes tracked from stations R0 through R3 (Figure 28) qualitatively appear fairly similar. The slope between these stations is steep but smooth and unvegetated, likely leading to slightly steepening wave heights as the water depth decreases onshore.

Meanwhile, the smaller ship wakes generally did not have the same initial distinct drawdown and surge seen in the ship wakes from larger cargo ships. It appears that the identified initial peak of the smaller ship wakes was a crest for roughly half of the time and a trough for roughly half of the time. Some smaller ship wakes that fell below the large ship threshold followed slightly different patterns; these likely correspond to far away cargo ships passing on the east side of the island (such as in Figure 23).

3.6 Wave Energy Estimations

The energy densities, energy fluxes, and wave heights at each station are compared for ship wakes and wind waves. The energy densities, energy fluxes, and wave heights at stations R0 through R3, which are on the unvegetated steeper slope, can be compared to those across stations R4 and R5, on the vegetated milder slope on peat platform. Patterns across the entire transect can also be considered.

First, energy flux averages and totals for all kept ship wakes found at station R0 are considered (Figure 30), as described in Chapter 2.3.

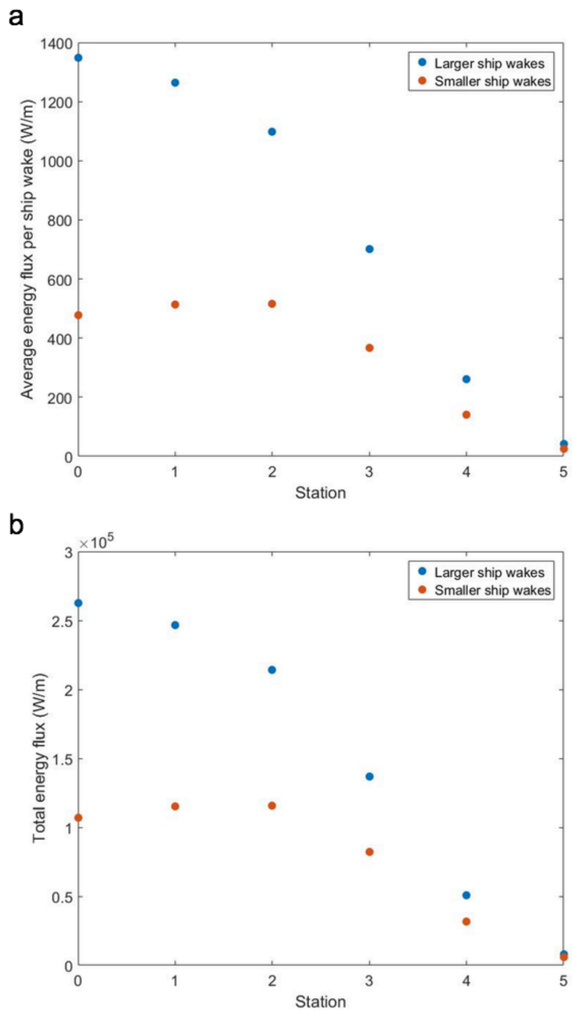

Figure 30: a) Average energy flux per ship wake across entire transect, from all ship wakes chosen from those identified at station R0; b) Total energy flux in ship wakes across entire transect, from all ship wakes chosen from those identified at station R0.

Energy flux averages and totals for the two other groups of ship wakes tracked across the unvegetated segment and across the entire transect were also estimated. The trends for the unvegetated stations R0 to R3, and for the entire transect R0 to R5, are shown for both larger ship wakes and smaller ship wakes in Figures 31 and 32.

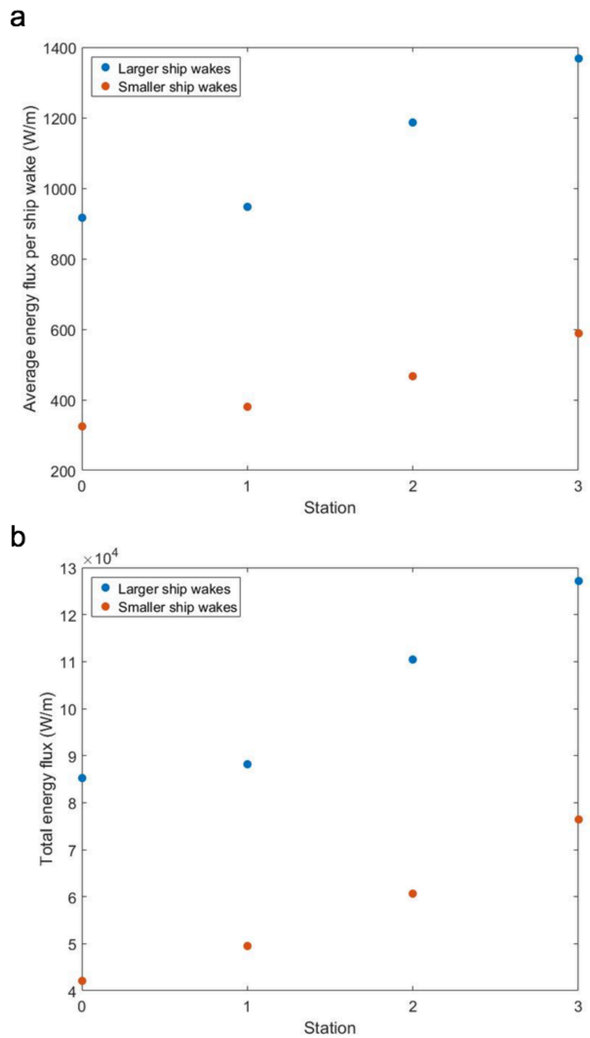

Figure 31: a) Average energy flux per larger ship wake tracked from stations R0 through R3; b) Total energy flux in larger ship wakes tracked from stations R0 through R3.

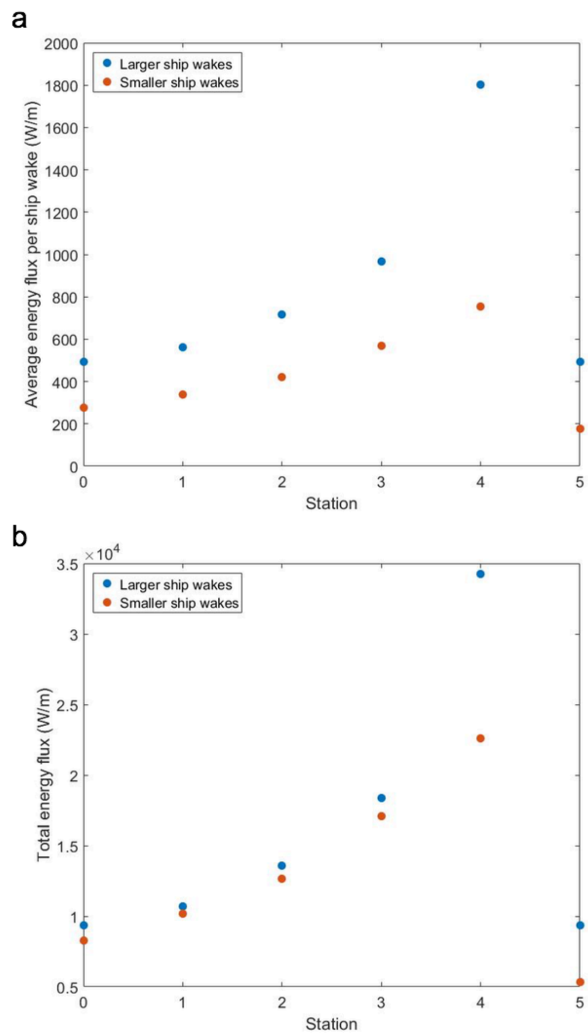

Figure 32: a) Average energy flux per large ship wake tracked from stations R0 through R5; b) Total energy flux in large ship wakes tracked from stations R0 through R5.

Total large ship wake energy fluxes decreased onshore across the transect (Figure 30) due to the higher water depths required to reach more landward stations. Small ship wake energy fluxes slightly increased onshore between stations R0 and R2, but the increases are likely within the noise of the measurements; energy flux appears to have been conserved between these stations. Station R2 was occasionally dry during lower tides, but still at a point where most ship wakes probably still reached it. One possibility for the differences between large and small ship wakes is the proximity and tracks of the smaller ships, such as the ferry, relative to the transect. Bottom friction may affect small ship wakes the most once the waves pass station R2, but before station R2 small ship wakes may experience little energy dissipation. Meanwhile, the large ship wakes entering shallower depths may experience higher levels of bottom friction. Large and small ship wakes may break at different locations, due to differences in wave steepness. In shallowing water, nonlinear effects may also contribute to the differences in total energy flux trends for large and small ship wakes.

Total and average energy fluxes estimated from all kept large and small ship tracked to station R3 increased onshore (Figure 31). Energy flux should be conserved or dissipated through wave breaking or friction. Possible reasons for the increase are that data were collected along a single cross-shore transect, and ship wakes likely refracted along the edge of the island. Wave rays could narrow as ship wakes moved onshore, increasing the energy density and thus the energy flux. The varying wave angles of ship wakes as a ship traveled by Pea Patch Island could increase the wave energy flux at one station over another. This effect cannot be fully quantified without the use of additional transects.

The number of ship wakes for comparison across the entire transect is a small fraction of the overall number of identified ship wakes due to the long periods of time that stations R4 and R5 were dry. For ship wakes tracked across the entire transect, energy density and energy flux totals increased from stations R0 to R3, rose more sharply at station R4, and then dropped sharply at station R5 (Figure 32). The energy fluxes likely increased for the same reasons discussed for the energy flux trends shown in Figure 31. Another possible contributing factor is that ship wakes only reached stations R4 and R5 during higher tides, which could affect how wave orbitals traveled; the higher water levels may decrease the amount of bottom friction. Even with the peat platform and the short patch of *Schoenoplectus pungens*, the energy fluxes still increased from station R3 to station R4. Reflection off of nearby peat platforms, as indicated in Chapter 3.3 (Figure 23e) could also contribute to a higher energy flux at station R4 than the other stations. The *Phragmites australis* attenuated the wave energy between stations R4 and R5. Waves may also have been breaking across the peat platform due to the sudden decrease in water depth. The average smaller ship wake energy fluxes were generally less than the corresponding average larger ship wake energy fluxes (Figure 32). Yet, due to the higher number of smaller ship passages, the smaller ship wake energy flux totals were close to the larger ship wake energy flux totals. As such, smaller ship wakes should not necessarily be entirely discounted.

Meanwhile, the wind wave energy density and energy flux totals increased from station R0 to station R2 and then dropped at stations R3, R4, and R5 (Figure 33). The study site on the western side of Pea Patch Island may be at least somewhat sheltered from wind by the ferry dock and the protruding eastern corner of the island. These factors could limit the fetch and growth of wind waves before they reach the site. Changes in wind direction would also limit the amount of wind energy transferred to waves. The wind energy fluxes increase from stations R0 to R2 appear more pronounced than the trend for smaller ship wakes that affected station R0 in Figure 30. The increases could be due to wind continuing to impart energy to the waves. Wind waves could hit station R2 more directly than stations R0 and R1. Station R3 is more sheltered and higher in elevation than stations R0 through R2, so fewer wind waves may reach it. Waves of greater height would have a higher chance of breaking and dissipating energy than waves of lower height. The cycle of high tides, low tides, spring tides, and neap tides affect how water depths change over time, thereby effecting how, where, or even if certain waves break.

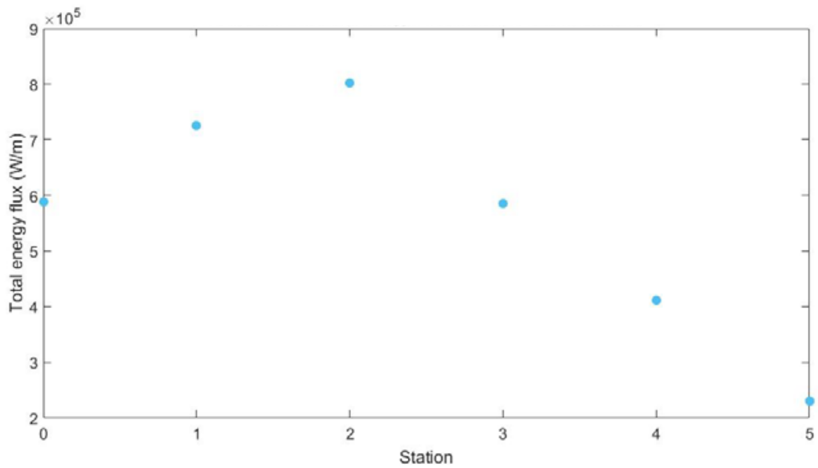

Figure 33: Total wind wave energy flux from stations R0 through R5.

The common factor between stations R3 and R4 is the peat platform edge. The edge introduces a discontinuity in the transect slope, providing a mostly impermeable barrier to water. During low tides when the mean water level is below the height of the platform, some incoming water may be absorbed (transmitted) into the peat soil, but most waves are either reflected or dissipated by the peat platform edge. The reflected waves may interact constructively or destructively with incoming ship wakes and wind waves. During high tides when the mean water level is above the height of the platform, waves may carry onto the platform but soon break due to the abrupt approximately 1-m decrease in water depth. The existence of the peat platform edge itself, in addition to the uneven geometry and rough texture of the peat platform edge (Figure 34), may intercept wave orbitals and slow down the wave, or introduce more nonlinearities. These nonlinearities perhaps cannot be captured by the linear wave theory equations used for energy density and energy flux.

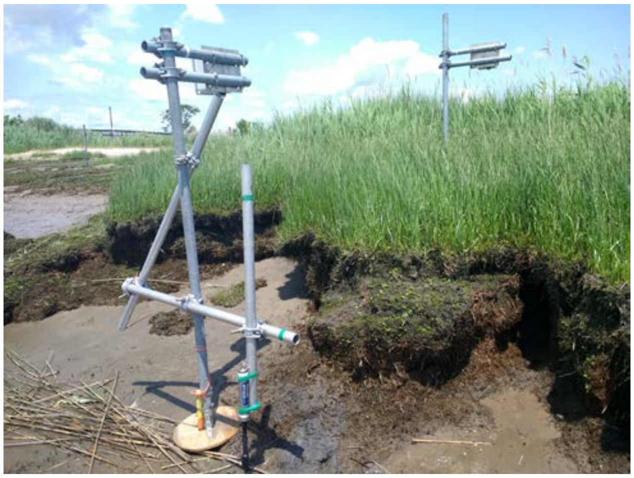

Figure 34: Close-up photograph of peat platform face between stations R3 and R4.

The waves reflected off of the peat platform face likely carry some of their incident wave energy back offshore toward station R3 and R2. Waves could reflect at oblique angles, especially due to the uneven and rough features of the peat platform face. Wave reflection could reduce the estimated wave energy flux at station R3.

The higher energy totals in ship-generated waves at station R4 (Figure 32) could be at least partially due to the aforementioned alongshore travel of wave energy reflected off of nearby peat platform edges. The leading waves of a ship wake train may carry higher energy than wind waves over a similar period of time, with higher ability to continue over the peat platform through the short *Schoenoplectus pungens* patch and reach station R4. The attenuation ability of the *Schoenoplectus pungens* is difficult to quantify due to the presence of the peat platform, but the high stem density may more effectively attenuate the higher-frequency wind wave energy than ship wake energy.

It must be emphasized that for this analysis, only ship wakes that reached R5 were considered for effective comparison across the transect in Figure 32. At the same time, even if all ship wakes found at station R0 were used (as in Figure 30), it would not be as useful because ship wakes during low tides are not as impactful as ship wakes during high tides. Similarly, storm events during low tides would not be as impactful as storm events during high tides. High tide combined with storm surge could damage the vegetation.

While a large ship wake may momentarily splash on top of the platform during lower tides, the vegetation does not experience continued wave action until the water level exceeds the peat platform height. Repeated wave attack on the peat platform edge may cause gradual erosion of the scarp structure. There was evidence from instrument height measurements of sediment shifting near R3 and being pushed against the peat platform. Yet the survey data show little to no morphological change over the month. This could be due to different operators placing the survey rod at different spots at the peat platform face. Change to the peat platform face may also occur over time periods greater than one month.

Aerial imagery of western Pea Patch Island in Figure 35 shows a gradual recession of the shoreline over time since 2002. It is not known at which tidal levels the photographs were taken, but the progression of images indicates definite changes. The banks of the creek to the right of the images erode and the creek widens over time. In the 2016 image, the most recent one available, the vegetation patch of interest is circled. It appears as a prominent marsh neck. From 2002 through 2016, it appears that the shoreline is migrating landward. Different tidal phases could reduce the effectiveness of comparing the images, but wetlands and shoreline recession can be seen using the ferry dock as a reference.

Figure 35: Aerial imagery over time of western Pea Patch Island wetlands near ferry dock: a) 2002 image showing a fairly straight shoreline and small creek to the right; b) 2005 image showing an increased shoreline perturbation near the ferry dock; c) 2010 image showing a mostly straight shoreline with a widening creek to the right; d) 2016 image showing an eroded and uneven shoreline with the vegetation patch of interest, and a widening creek to the right.

Water runs farther up the beach slope in the adjacent bare areas near the vegetation patch of interest, allowing for greater erosion due to ship wakes during low and high tides than along the transect of interest. This effect is evident in Figure 36, where the vegetation patch stretches farther into the water relative to the adjacent unvegetated beach area. The area adjacent to the vegetation patch could be considered a cleft in the marsh shoreline.

Figure 36: Photograph of study site and adjacent unvegetated area.

It is possible vegetation farther onshore of the unvegetated area next to the vegetation patch was cleared or eaten by animals (Figure 37). The uniform nature of the cut relative to the tall vegetation on the platform indicates the stems may have been cut by humans. There appears to be small and short areas of peat as well, on which some young *Schoenoplectus pungens* were growing. The circled marsh stack in Figure 37 indicates that at one point the peat platform extended farther into the river and in the direction of the cleared area. If the peat platform did extend farther alongshore, it would likely provide better attenuation of waves and protection of the landward shore. However, as it is now, the peat platform is essentially becoming a headland, on which waves may converge through refraction and diffraction.

Figure 37: Photograph of cut vegetation and sparse peat next to vegetation patch of interest. The circled feature is a marsh stack, a separated part of the peat platform.

Considering energy fluxes from ship wakes and wind waves, at station R0 ship wakes contributed about 39% of the total energy flux and wind waves contributed about 61% of the total energy flux. The relative contribution of wind wave energy increased onshore across the transect as the relative contributions of large and small ship wake energy decreased (Figure 38). The relative contributions of large and small ship wakes at stations R4 and R5 appear approximately even, as indicated in Figure 32b.

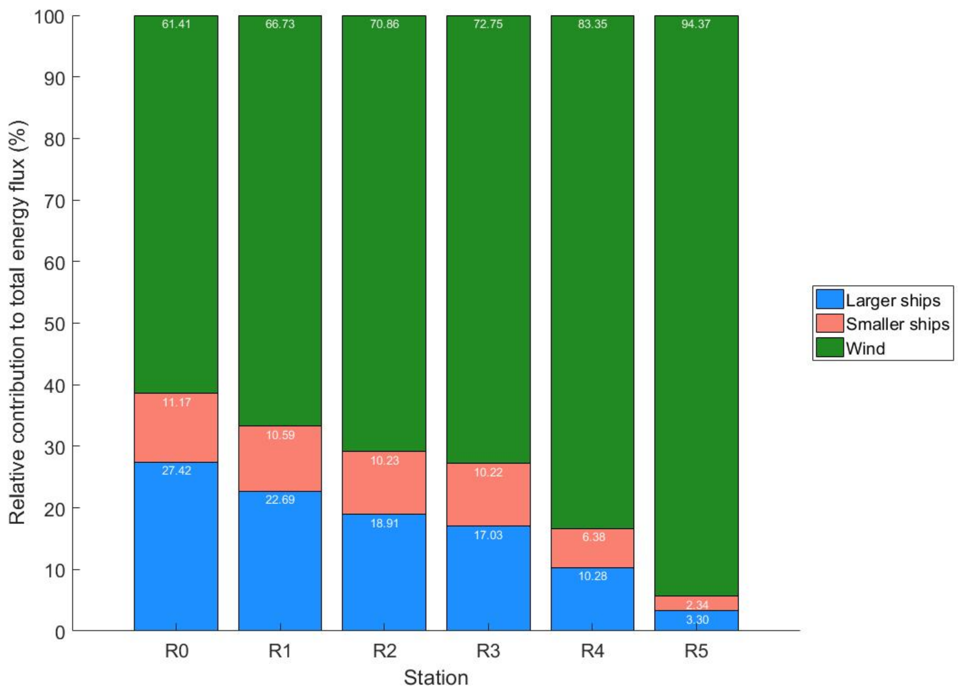

Figure 38: Relative contributions of ship- and wind-generated waves to total energy flux across the entire transect.

The vegetation may more effectively attenuate ship wakes than wind waves. Perhaps wind blowing across the peat platform continues to transfer energy to waves, even as the vegetation physically blocks the wind. The *Phragmites australis* density is low relative to the *Schoenoplectus pungens*, allowing more space for wind to influence waves. As drag depends on fluid density, the shear stresses between the stem surfaces and wind forces (air) may not induce as much drag on the wind as the shear stresses between the stem surfaces and ship wakes (water) induces on waves.

Hofmann et al. (2008) compared the effects of wind- and ship-generated waves on Lake Constance in Europe and found that, over the entire year, wind waves contributed about 50% of the mean annual energy flux and ship wakes contributed about 41% of the mean annual energy flux, excluding wave heights below 0.05 m. They found ship wakes contributed about 50% of the energy flux in summer and about 35% of the energy flux in winter. They also found that wind wave energy fluxes were highly variable from month to month. The relative contributions between wind- and ship-generated waves at Pea Patch Island during the summer appear similar to the results described by Hofmann et al. (2008) during summer. Some of the sites studied on Lake Constance may experience more summer boat traffic than the western side of Pea Patch Island.

The results indicate that in late spring to early summer, ship wakes have comparable impact relative to wind waves on the initial unvegetated cross-shore face, but little impact relative to wind waves on areas in the peat platform. During this time period, the accumulated wind wave power probably contributes the most to erosion of the peat platform face and area landward of it. During this time period, the accumulated wind wave power and ship wake power comparably contribute to erosion of the unvegetated slope.

It must be noted that, as the study was conducted during June and July, from late spring to early summer, winds may not have been as strong as in winter. Further, the Delafort ferry runs only for special events outside of the main warmer visiting season, reducing the impact of smaller ship wakes on the island in colder months. Assuming consistent schedules, larger cargo ships would still pass by the island. Some larger passenger ships, such as the *Kalmar Nyckel* (which was observed at Pea Patch Island during the experiment), may stop passing the island in winter, but such ships are likely not heavily loaded with cargo and may not generate high-energy wakes. In winter time, due to higher winds, more storms, and fewer small ship wakes, wind energy would likely dominate more.

The ship wake energy fluxes are delivered in more concentrated packets relative to accumulated small wind waves. To estimate the hypothetical total ship wake energy flux over the entire study, one could divide the total ship wake energy by the total time duration of the identified ship wakes and multiply that quotient by the total record time duration. In this case, at station R0 if the ship wake energy flux total was applied across the period June 7 through July 7, 2019, it would exceed the wind wave energy flux total by a factor of about 5.2. At station R1, this hypothetical extended ship wake energy to wind energy factor would be about 4.1, at station R2, about 3.4; at station R3, about 3.1; at station R4, about 1.7; and at station R5, about 0.5.

The low-frequency and high-frequency significant wave heights in each large (Figure 39) and small (Figure 40) ship wake tracked to stations R4 and R5 were compared.

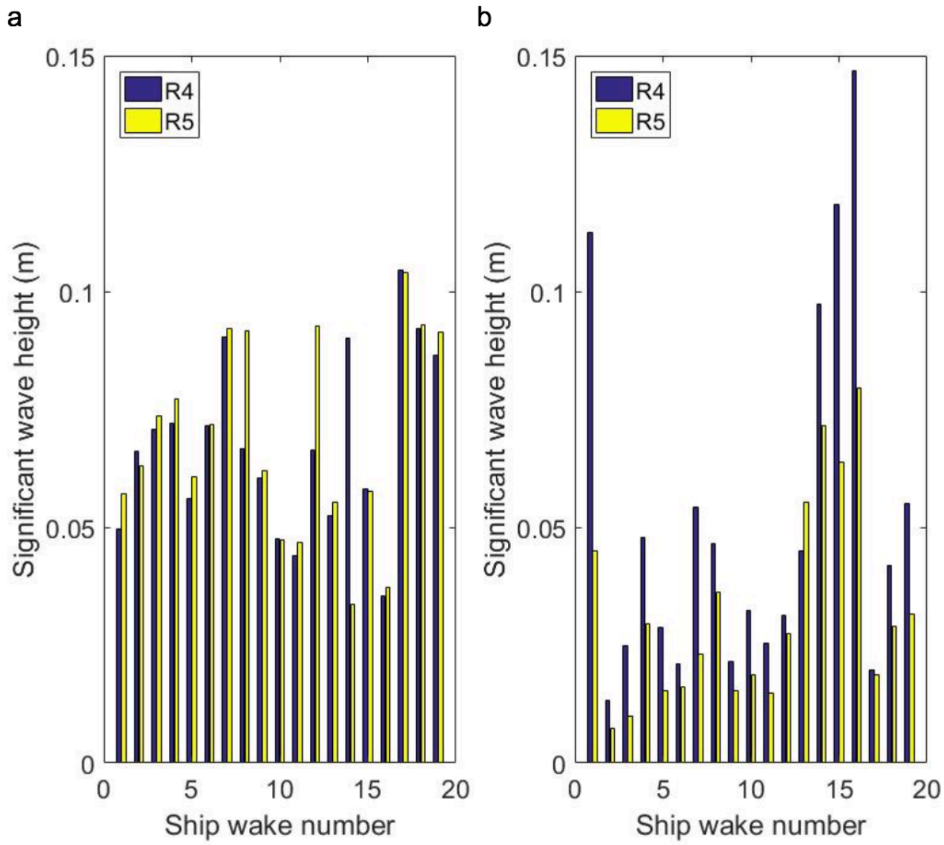

Figure 39: a) Low-frequency significant wave heights of each large ship wake tracked to stations R4 and R5; b) High-frequency significant wave heights of each large ship wake tracked to stations R4 and R5.

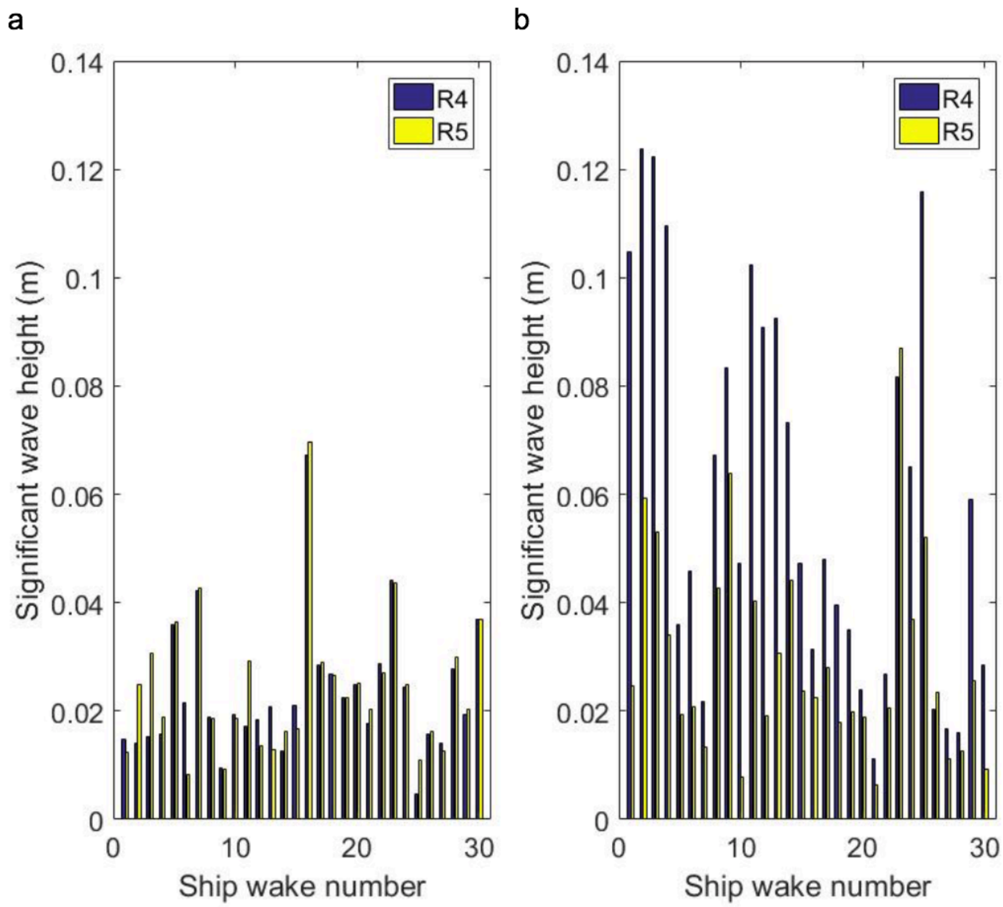

Figure 40: a) Low-frequency significant wave heights of each small ship wake tracked to stations R4 and R5; b) High-frequency significant wave heights of each small ship wake tracked to stations R4 and R5.

The low-frequency wave heights saw little to no reduction between stations R4 and R5. The low-frequency significant wave heights sometimes increased between stations R4 and R5, which could be due to differences in wavelength and group velocity among low-frequency wave components of ship wakes. Oblique low-frequency waves generated by ships turning or passing the southwestern corner of Pea Patch Island may have greater effect on station R5 than R4. The high-frequency wave heights consistently drop between stations R4 and R5, likely because high-frequency waves are more easily damped out by friction. The *Phragmites australis* patch had thick stems but relatively low stem density, interrupting wave crests and making waves more short-crested and three-dimensional than long-crested and two-dimensional. The *Schoenoplectus pungens* patch was denser but the stem diameters were smaller. While smaller diameters individually likely have less impact on wave crests, the stem density likely also interrupted the wave crests.

The relative reductions of low-frequency and high-frequency wave heights through vegetation appears to match the finding by (Anderson and Smith, 2014) that vegetation more effectively attenuates higher frequency wave components than lower frequency wave components.

The percentage reduction of total energy flux between stations R4 and R5 for large and small ship wakes tracked to stations R4 and R5 were compared (Figure 41).

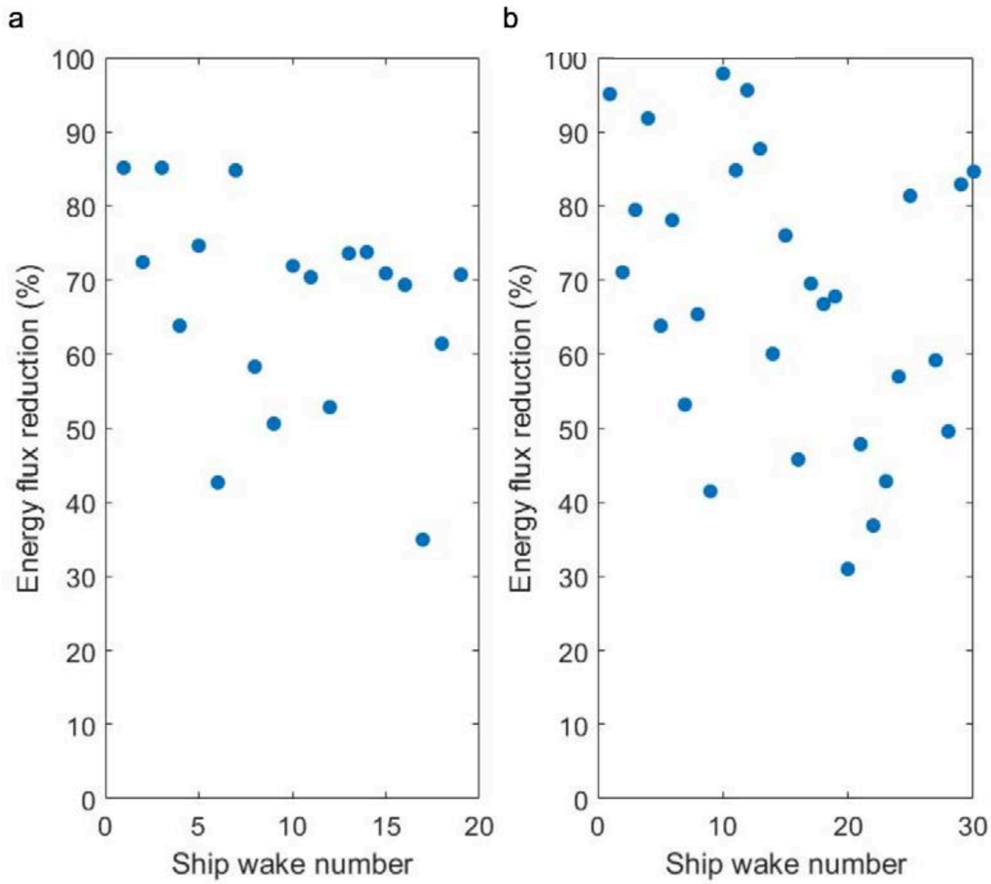

Figure 41: a) Energy flux percentage reductions for large ship wakes between stations R4 and R5; b) Energy flux percentage reductions for small ship wakes between stations R4 and R5.

There was at least 30% ship wake energy flux reduction between stations R4 and R5 for ship wakes tracked to stations R4 and R5. Some small ship wakes experienced almost 100% energy flux reduction, which could have occurred at a tidal level where water barely reached station R5. No larger ship wakes tracked to stations R4 and R5 appeared to experience more than 90% energy flux reduction. However, at that point wave energy would be so low as to have little to no impact. The *Phragmites australis* was likely predominantly responsible for this attenuation, in combination with gravity and bed shear stress to a lesser extent. Smaller ship wakes generally had lower low-frequency wave heights, which could account for the higher levels of dissipation for smaller ship wakes relative to larger ship wakes. Meanwhile, the *Phragmites australis* reduced the average wind wave energy flux by about 22%.

Analyses can also be done in the frequency domain, for which wave spectra are needed. The wave energy is represented by the area under the spectrum divided by the fluid density and acceleration due to gravity (Kamphuis, 2010). Power spectra are determined by a number of parameters that can affect the resolution and accuracy of the results.

3.7 Additional Observations of Ship Wakes at Study Site

It would be useful to consider these data in combination with qualitative observation of an individual ship wake train. In Figure 42a, the oblique wave crests of a ship wake train appear to be refracting, likely due to the steep increase in water depths offshore indicated by survey data. Figure 42b shows multiple successive wave groups arriving onshore at the study site in a train. There appear to be smaller waves propagating roughly perpendicularly to the ship wakes, perhaps due to wind or momentum transfer as the waves in the ship wakes break at an angle oblique to the shoreline.

Figure 42: Snapshots of a ship wake at the study site, taken on April 20, 2018: a) View of refracting ship wake arriving onshore; b) View of ship wake train arriving onshore.

3.8 Sediment at Study Site

It is also important to consider the sediment at the study site. The nature of the sediment changed over the length of the transect of interest. At stations R0, R1, and R2, the sediment was cohesive but mostly inorganic. Organic content increased in the onshore direction. Station R3 sediment showed more organic content than that at Stations R0, R1, and R2, while stations R4 and R5 showed even greater levels of organic content, likely of the Broadkill Mucky Peat type indicated in Figure 4. The root systems are deeply embedded in and intertwined with clays and silts at stations

R4 (Figure 43) and R5. Some of the organic material appeared to be at different stages of decomposition. The less decomposed material likely offered higher binding strength for plant roots.

Porous peat soils may saturate more easily than soils with less organic content. Saturation of soil along the transect could affect wave parameters and wave energy dissipation through water infiltrating into the soil. Differences in water content and porosity of soil across the transect could lead to gradients in saturation, pore pressures, and the effects of infiltration on waves.

Figure 43: Photograph of sediment cored from station R4 scaffolding pipe.

Chapter 4

CONCLUSIONS AND FUTURE WORK

4.1 Findings

Data from a field study conducted during the summer of 2018 on Pea Patch Island were collected, processed, and analyzed to explore the impacts of wind- and ship-generated waves on the island and the effectiveness of vegetation in attenuating these waves.

Identified larger ship wakes had a characteristic and distinctive initial drawdown and surge. Identified smaller ship wakes had initial peaks but mostly lacked the obvious drawdown and surge pattern. Occasionally ships passed the island simultaneously or in quick succession; while these ship wakes were removed from the analyses, the potentially superimposed waves could have higher wave energy fluxes and thus greater erosive impacts on the island.

For all identified ship wakes at station R0, the average and total large ship wake energy fluxes had similar relationships to the average and total small ship wake energy fluxes, respectively. Even though there were more smaller ship wakes, overall the energy fluxes contained in larger ship wake were greater than energy fluxes contained in smaller ship wakes.

For the ship wakes tracked through station R5, in other words during higher tides, the average larger ship wake energy fluxes were greater than the average smaller ship wake energy fluxes, but the total large ship wake energy fluxes were almost the same. Thus the effects of smaller ship wakes should not be neglected; while the individual erosive effects of smaller ship wakes may be smaller than those of larger ship wakes, the higher numbers of smaller ship wakes may compensate, at least during higher tides. The small sample size may also have had an effect on this comparison.

Wind increasingly contributed more to total energy fluxes across the transect relative to large and small ship wakes during this late spring to early summer study. Yet the ship wake energy fluxes were more highly concentrated in finite packets. Sudden increases in the number of ships passing the island could increase the erosive impact of ship wakes even more. During winter, it is expected that the relative contributions of wind would be even greater due to storms and fewer ship passages.

Considering the ship wakes tracked across the entire transect, the *Phragmites australis* attenuated wave energy, as wave energy flux totals decreased between stations R4 and R5. Percentage wave energy flux reductions varied between 30% and 90% for larger ship wakes and between 40% and nearly 100% for smaller ship wakes. The *Phragmites australis* more effectively attenuated higher frequency wave heights and lower frequency wave heights.

It was difficult to analyze wave attenuation by the *Schoenoplectus pungens* between stations R3 and R4 due to the peat platform. It is possible wave energy reflected off of nearby peat platforms intersected with station R4. Wave energy reflected off of the peat platform in the transect likely affected station R3 the most. The nonlinearities introduced by wave refraction, reflection, and water travelling through vegetation introduced additional complexities.

4.2 Implications for DNREC and Pea Patch Island

4.2.1 Vegetation

This study can be useful to DNREC in several ways. It can make the agency more aware of the ability of *Phragmites australis* to attenuate waves, showing the plant has ecological benefits and is not merely a weed to be eliminated. The dataset and analyses may be of use in the future to the United States Army Corps of Engineers, especially for dredging or other engineering projects in the vicinity of Pea Patch Island.

DNREC has a program to eradicate invasive *Phragmites australis*. Such programs are usually implemented to create space for other species to grow, increasing biodiversity and improving animal habitats. Yet clearing swaths of the invasive reed leaves the ground bare and unprotected, making the inland areas more vulnerable than before to wind waves, ship wakes, and storms. In addition, Parsons (2003) conducted a study on Pea Patch Island that showed some wading bird species had higher success nesting among *Phragmites australis* than in upland areas, and stands of the tall reeds could protect wading birds from visitors and unauthorized boat landings. Clearing these stands could conceivably harm rather than help some of the bird populations on the island.

In addition, Rooth and Stevenson (2000) found higher rates of organic material and mineral accumulation in *Phragmites australis* communities than in *Spartina* communities in a subsiding creek bank marsh and a laterally eroding marsh, both in the Chesapeake Bay. The *Spartina* communities were denser than the *Phragmites australis* communities, so the authors attributed the increased depositional pattern to *Phragmites australis* litter accumulation and higher below-ground growth.

While invasive *Phragmites australis* can push out native plant species and reduce plant biodiversity, they can still be habitats amenable to wildlife. Removal of invasive *Phragmites australis* could increase erosional effects on Pea Patch Island and other areas where the invasive reed is dominant. Even if a different plant species is used to replace *Phragmites australis* after clearing, the plant may not have the same level of wave attenuation ability. Resultant erosion and sea level rise could potentially overwhelm the plant, accelerating wetlands loss. This is not to suggest replanting *Phragmites australis* is universally a good solution; there may be native plants similar enough to do the same job. Native *Phragmites americanus* could also be used to increase coastal protection, while allowing other plant species to coexist in biodiverse communities, but it should not be assumed *Phragmites americanus* has the same wave attenuation ability and salinity tolerance as *Phragmites australis*.

Programs aimed at clearing *Phragmites australis* may involve the destruction of the peat platforms they stand on, due to the extensive rhizome systems of the plant. The allowed continued accretion of peat platforms and establishment of more peat platforms could help protect Pea Patch Island against future local sea level rise. This may need to be combined with construction of additional embankments or protective earth walls.

4.2.2 Ship Wakes

While decreasing caps on ship speeds could help reduce the impacts of ship wakes on Pea Patch Island, the negative effects on commerce may not be worth it. There are several ship design techniques that can reduce the generation and impact of ship wakes. One example is the bulbous bow, an underwater feature protruding underwater at the bow of a ship. Initially used as a weapon in war, the bulbous bow was found to be useful in partially canceling out waves, thereby reducing wave resistance and increasing efficiency (Ferreiro, 2011). Many but not all larger cargo ships currently employ the bulbous bow.

Limiting the distance between ships and the island could help reduce the incident wave power due to bottom friction and wave energy dissipation exerted over greater distances. However, due to the limited width of the Delaware River, it would not be feasible to require ships to maintain a certain distance from the island. In doing so, ships may pass closer to Delaware or New Jersey, increasing potential impact on those shorelines. Large cargo ships need wide berths to pass each other, and would not veer into shallower waters.

For increased coastal protection against ship wakes, hardened coastal armoring such as riprap can effectively reflect ship wake energy, at the cost of alongshore sediment transport and natural inundation of wetlands. Hybrid porous coastal armoring techniques, such as using coir logs, are more natural options that dissipate wave energy without as many adverse effects.

4.3 Improvements and Future Work

Multiple improvements could be made to the data collection, processing, and analyses. Due to the financial and logistical difficulties of returning to Pea Patch Island every day, especially in the presence of tour groups and events, not all instruments could collect continuous high-resolution data. All of the ADV data and some of the ECM data were collected in burst mode. The UDMs were run at 2 Hz for most of the study, and at 4 Hz for the rest.

Running the Vector in continuous mode would have demanded frequent downloads of data and replacements of batteries. That would have required either a different setup, which may have been difficult with the low water levels relative to the instrument blanking distance, or removing and reinstalling the heavy mount out of the water at every visit. Running the ECMs at 5 Hz meant batteries had to be replaced every two to three days, which is especially not viable considering weekends. Sampling rates of 2 Hz and 4 Hz are likely not adequate for resolving complicated wave signals, leading to loss of resolution and accuracy in results. Increasing the UDM sampling rate would also require more frequent trips to the island. Furthermore, pressure sensor batteries should be swapped out at least once every two weeks; even though the program gave an estimated of over 80 days of battery life, the batteries of some pressure sensors started to experience issues in the last day of the study, leading to lost data.

Using pressure sensors instead of UDMs at stations R4 and R5 may possibly have provided cleaner, more accurate data sets that were easier to process and work with. On the other hand, pressure data must be converted to water depths and pressure gauges may not capture all frequency components in shallow water depths.

As vegetation biomass changes throughout the year, multiple studies would have been preferred to gauge differences in vegetation-induced attenuation of wave energy. Indeed, the vegetation patch of interest changed between the preliminary visit to Pea Patch Island in April, 2018 and the study in June to July, 2018. The patch of *Schoenoplectus pungens* at the edge of the peat platform was nonexistent in April. In fact, *Phragmites australis* and *Schoenoplectus* grew over the course of the study. At the start of June, *Schoenoplectus pungens* was unidentifiable due to not bearing any seedheads yet. As the month went on, seedheads started appearing on the stems. As mentioned before, tiny plants also began growing in the cleared area around stations

R4 and R5 as sunlight infiltrated to the ground (Figure 44). These plants were actively removed but kept returning. They may cause noise in the water depth data near low tide with regard to the location of the bed level, but they were removed frequently enough so as not to cause a problem. Such vegetation growth may be nonexistent in winter.

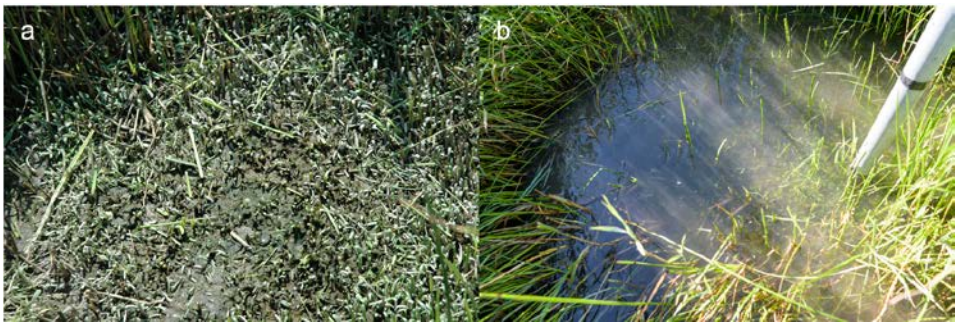

Figure 44: a) Photograph of plants growing in cleared areas near scaffolding pipes during the study; b) Photograph (taken by Evan Krape) of *Schoenoplectus pungens* near station R4 that regrew in between visits. Photographs of plants growing in cleared areas near the scaffolding pipes at stations R4 and R5 during the study.

Conducting longer-term studies or multiple studies throughout the year could also help distinguish potential seasonal changes in vessel- and wind- generated wave patterns. Long-term studies would also increase the sample size of ship wakes tracked to stations R4 and R5, allowing for more detailed and accurate comparisons.

Adding more data collection stations within the vegetation patch could have provided a better resolution of how wave height reduction changes as a function of distance and time. Station R5 was not at the most landward edge of the vegetation patch because the vegetation extended far inland, into a swampy area that could have been risky to deploy instruments in. Beyond station R5, noticeable increases in wave height reduction relative to that occurring between stations R4 and R5 are not likely.

Velocity data recorded in the vegetation patch would have provided more opportunities for quantitative analysis of vegetation-induced wave attenuation, but not enough current meters were available. A velocity profiler could provide some additional information on how the velocity changes with depth. These velocity data, in combination with measured vegetation characteristics, could be tested against models of flow velocities through vegetation and be used to estimate drag and turbulent kinetic energy.

Several numerical models exist to predict flow fields through vegetation. Numerical models could be calibrated with site measurements, and predictions could be compared against the actual data. For this purpose, it may be helpful to do the aforementioned control study with two parallel transects, one in a vegetated area and one on adjacent unvegetated beach with similar cross-shore slopes (except for the peat platform discontinuity).

The peat platform edge, while a ubiquitous feature in coastal wetlands and salt marshes, complicated data processing and analysis. The peat platform edge itself could be the subject of future study, as it essentially presents a hard obstacle to the flow field as waves begin to enter the vegetation.

Sediment concentration or turbidity data could provide more insight into impacts of wind- and vessel-generated waves and vegetation-induced attenuation of waves. As mentioned before, instruments were not deployed to collect such data because of the murkiness of the water, the abundance of suspended plant material that may have interfered with measurements, and the difficulty in accurate calibration.

In hindsight, deploying an anemometer to measure wind speeds and directions throughout the month would have been helpful in analyzing wind-generated waves, instead of using data from a nearby airport. Using an anemometer would have allowed for a higher accuracy and resolution of wind data. Nearby weather stations and airports may have anemometers, but these do not well represent the localized wind speeds and directions over the water near the study site.

Frequency domain analyses can be improved to better distinguish between wind waves and ship wakes, in particular between wind waves and smaller ship wakes. Any such analyses should take into account the fact that wind events of varying strength occur throughout each day. Stronger wind events could potentially mask spectral peaks corresponding to ship wakes (Hofmann et al., 2008). Frequency domain analyses could also be used to compare energy estimates derived from power spectra with energy estimates derived from time domain analyses.

The time lapse camera at the western site was tipped slightly to the side multiple times by birds during the first week of the deployment. At the eastern site, a bird caused the time lapse camera to flip forward completely, losing several days of imagery. More tightly securing the housing to the mount helped avoid this issue for the rest of the study. In future studies on Pea Patch Island or at other areas with high bird populations, bird-resistant housing could be implemented to help prevent this issue. Similarly, measures should be taken to protect sensors from birds and ensure bird waste cannot impact sensor probes.

The energy flux reductions across the transect and between stations R4 and R5 can be at least roughly categorized by point in the tidal cycle, ship type, ship size, and ship weight to identify common trends. The Froude number could also be estimated for ship wakes to identify possible trends between ship, wave, and tidal parameters.

Beyond the improvements discussed above, there is still room for more work on Pea Patch Island and in wetland areas in general. Remote sensing and imaging, such as infrared imaging or synthetic-aperture radar, could be used to better visualize the interaction of vessel-generated waves with Pea Patch Island. Long-term monitoring of the wetlands could yield approximate peat accretion rates as well as erosion and retreat rates, which could be related to wind- and ship-generated energy flux changes.

REFERENCES

Ache, B. W., Crossett, K. M., Pacheco, P. A., Adkins, J. E., & Wiley, P. C. (2015). “The Coast” is Complicated: A Model to Consistently Describe the Nation’s Coastal Population. *Estuaries and Coasts*, *38*, 151–155. https://doi.org/10.1007/s12237-013-9629-9

Anderson, M. E., & Smith, J. M. (2014). Wave attenuation by flexible, idealized salt marsh vegetation. *Coastal Engineering*, *83*, 82–92. https://doi.org/10.1016/j.coastaleng.2013.10.004

Chatagnier, J. (2012). *The biomechanics of salt marsh vegetation applied to wave and surge attenuation*.

Coxe, R. (2012). *Historical analysis and map of vegetation communities, land covers, and habitats of Fort Delaware State Park New Castle County , Delaware*.

DeLaune, R. D., & White, J. R. (2012). Will coastal wetlands continue to sequester carbon in response to an increase in global sea level?: a case study of the rapidly subsiding Mississippi river deltaic plain. *Climatic Change*, *110*(1–2), 297–314. https://doi.org/10.1007/s10584-011-0089-6

Delaware River main channel deepening project: supplemental environmental impact statement. (1997). https://doi.org/10.1016/0003-6870(73)90259-7

Delaware River main channel deepening project USACE responses to questions from the DNREC Hearing Officer provided July 27, 2010. (2010).

Delaware River main stem and channel deepening project environmental assessment April 2009. (2009).

Fang, M. C., Yang, R. Y., & Shugan, I. V. (2011). Kelvin ship wake in the wind waves field and on the finite sea depth. *Journal of Mechanics*, *27*(1), 71–77.

Feagin, R. A., Figlus, J., Zinnert, J. C., Sigren, J., Martínez, M. L., Silva, R., … Carter, G. (2015). Going with the flow or against the grain ? The promise of vegetation for protecting beaches, dunes, and barrier islands from erosion. *Frontiers in Ecology and the Environment*, *13*(4), 203–210. https://doi.org/10.1890/140218

Ferreiro, L. (2011). The Social History of the Bulbous Bow. *Technology and Culture*, *52*(2), 335–359.

Gedan, K. B., Kirwan, M. L., Wolanski, E., Barbier, E. B., & Silliman, B. R. (2011).

The present and future role of coastal wetland vegetation in protecting shorelines: Answering recent challenges to the paradigm. *Climatic Change*, *106*(1), 7–29. https://doi.org/10.1007/s10584-010-0003-7

Gharbi, S., Hamdi, S., Valkov, G., & Nistor, I. (2008). Field measurements of ship waves along the St. Lawrence river waterway, Canada. In *OCEANS* (pp. 1–10).

Herbert, D., Astrom, E., Bersoza, A. C., Batzer, A., McGovern, P., Angelini, C., … Sheremet, A. (2018). Mitigating erosional effects induced by boat wakes with living shorelines. *Sustainability*, *10*(2), 436. https://doi.org/10.3390/su10020436

Hofmann, H., Lorke, A., & Peeters, F. (2008). The relative importance of wind and ship waves in the littoral zone of a large lake. *Limnology and Oceanography*, *53*(1), 368–380.

James, C. S. (2004). Flow resistance of emergent vegetation. *Journal Of Hydraulic Research*, *42*(4), 390–398. https://doi.org/10.1080/00221686.2004.9641206

Kamphuis, J. W. (2010). *Introduction to Coastal Engineering and Management* (2nd ed.). WORLD SCIENTIFIC. https://doi.org/10.1142/7021

Knutson, P. L., Brochu, R. A., & Seelig, W. N. (1982). Wave damping in Spartina alterniflora marshes. *Wetlands*, *2*(1), 87–104.

Lightbody, A. F., & Nepf, H. M. (2006). Prediction of velocity profiles and longitudinal dispersion in emergent salt marsh vegetation. *Limnology and Oceanography*, *51*(1), 218–228.

Luhar, M., & Nepf, H. M. (2013). From the blade scale to the reach scale: A characterization of aquatic vegetative drag. *Advances in Water Resources*, *51*, 305–316. https://doi.org/10.1016/j.advwatres.2012.02.002

Nepf, H. M. (1999). Drag, turbulence, and diffusion in flow through emergent vegetation. *American Geophysical Union*, *35*(2), 479–489.

Nepf, H. M. (2012). Hydrodynamics of vegetated channels. *Journal of Hydraulic Research*, *50*(3), 262–279. https://doi.org/10.1080/00221686.2012.696559

Nepf, H. M., & Vivoni, E. R. (2000). Flow structure in depth-limited, vegetated flow. *Journal of Geophysical Research*, *105*(C12), 28547–28557.

Neumann, B., Vafeidis, A. T., Zimmermann, J., & Nicholls, R. J. (2015). Future Coastal Population Growth and Exposure to Sea-Level Rise and Coastal Flooding - A Global Assessment. https://doi.org/10.1371/journal.pone.0118571

Parsons, K. C. (2003). Reproductive success of wading birds using Phragmites marsh and upland nesting habitats. *Estuaries*, *26*(2), 596–601.

Quartel, S., Kroon, A., Augustinus, P. G. E. F., Van Santen, P., & Tri, N. H. (2007). Wave attenuation in coastal mangroves in the Red River Delta, Vietnam. *Journal of Asian Earth Sciences*, *29*(4), 576–584. https://doi.org/10.1016/j.jseaes.2006.05.008

Rooth, J. E., & Stevenson, J. C. (2000). Sediment deposition patterns in Phragmites australis communities: Implications for coastal areas threatened by rising sea-level. *Wetlands Ecology and Management*, *8*(2–3), 173–183.

Schwimmer, R. A. (2001). Rates and Processes of Marsh Shoreline Erosion in Rehoboth Bay, Delaware, U.S.A. *Journal of Coastal Research*, *17*(3), 672–683.

Soomere, T. (2006). Nonlinear ship wake waves as a model of rogue waves and a source of danger to the coastal environment: A review. *Oceanologia*, *48*(S), 185–202.

Soomere, T., Parnell, K. E., & Didenkulova, I. (2009). Implications of fast-ferry wakes for semi-sheltered beaches: a case study at Aegna Island, Baltic Sea. *Journal of Coastal Research*, *56*(1), 128–132.

Tanino, Y., & Nepf, H. M. (2008). Laboratory Investigation of Mean Drag in a Random Array of Rigid , Emergent Cylinders, *134*(1), 34–41.

Titus, J. G. (1998). Rising Seas, Coastal Erosion, and the Takings Clause: How to Save Wetlands and Beaches Without Hurting Property Owners. *Maryland Law Review*, *57*(4).

Torsvik, T., Soomere, T., Didenkulova, I., & Sheremet, A. (2015). Identification of ship wake structures by a time – frequency method. *Journal of Fluid Mechanics*, *765*, 229–251. https://doi.org/10.1017/jfm.2014.734

Verney, R., Deloffre, J., Brun-Cottan, J., & Lafite, R. (2007). The effect of wave-induced turbulence on intertidal mudflats: Impact of boat traffic and wind. *Continental Shelf Research*, *27*(5), 594–612. https://doi.org/10.1016/j.csr.2006.10.005